Ice content and interannual water storage changes of an active rock glacier in the dry Andes of Argentina

Christian Halla[1], Jan Henrik Blöthe[1], Carla Tapia Baldis[2], Dario Trombotto[2], Christin Hilbich[3], Christian Hauck[3], Lothar Schrott[1]

5   [1]Department of Geography, University of Bonn, Bonn, 53115,
    [2]Instituto Argentino de Nivología, Glaciología y Ciencias Ambientales, CCT CONICET, 5500 Mendoza, Argentina
    [3]Department of Geosciences, University of Fribourg, Fribourg, 1700, Switzerland

Correspondence to: Christian Halla (chris.halla@uni-bonn.de)

10 **Abstract**

The quantification of volumetric ice and water contents in active rock glaciers is necessary to estimate their role as water stores and contributors to runoff in dry mountain catchments. In the semi-arid to arid Andes of Argentina, active rock glaciers potentially constitute important water reservoirs due to their widespread distribution. Here however, water storage capacities and their interannual changes have so far escaped quantification in detailed field studies. Volumetric ice and water

15 contents were quantified using a petrophysical four-phase model (4PM) based on complementary electrical resistivities (ERT) and seismic refraction tomographies (SRT) in different positions of Dos Lenguas rock glacier in the Upper Agua Negra basin, Argentina. We derived vertical and horizontal surface changes of the Dos Lenguas rock glacier, for the periods 2016–17 and 2017–18 using drone-derived digital elevation models (DEM). Interannual water storage changes of –36 mm yr^{-1} and +27 mm yr^{-1} derived from volumetric surface changes for the periods 2016–17 and 2017–18, respectively, indicate

20 that significant amounts of annual precipitation rates can be stored in and released from the active rock glacier. Heterogeneous ice and water contents show ice-rich permafrost and supra-, intra- and sub-permafrost aquifers in the subsurface. Active layer and ice-rich permafrost control traps and pathways of shallow ground water, and thus regulate interannual storage changes and water releases from the active rock glacier in the dry mountain catchment. The ice content of 1.7–2.0×10^9 kg in the active Dos Lenguas rock glacier represents an important long-term ice reservoir, just like other

25 ground ice deposits in the vicinity, if compared to surface ice that covers less than 3% of the high mountain catchment.

1 Introduction

Presently moving rock glaciers are classified as active rock glaciers (Barsch, 1996) that are defined as the *"the visible expression of cumulative deformation by long-term creep of ice/debris mixtures under permafrost conditions"* (Berthling, 2011, p. 105). Rock glaciers constitute predominant landforms in the extensive periglacial belts of arid high mountain

30 regions, such as the Central Andes of Argentina and Chile (Corte, 1976; Trombotto et al., 1999). Here, rock glaciers show some of the highest spatial densities worldwide (Azocar and Brenning, 2010; Blöthe et al., 2019), covering more surface area than glaciers in some parts (IANIGLA, 2018).

Besides storing large amounts of sediment, rock glaciers have been identified and discussed as significant water reservoirs in the dry Andes due to their widespread distribution (Arenson and Jakob, 2010; Brenning, 2010; Corte, 1976, 1978). Recently,

35 first order assessments of their water storage capacities suggest that significant amounts of ice are stored in rock glaciers (Jones et al., 2018a). However, field based studies that rigorously quantify rock glacier water storage capacities and their interannual changes are lacking in the region (Schaffer et al., 2019). In this study we investigate the water storage capacities of a tongue-shaped rock glacier, whose material source are periglacial talus slopes located on the valley side. It is beyond the scope of this case study to discuss the multiple hypothesis regarding the genetic evolution of rock glaciers (Knight et al.,

40 2019) and debate periglacial and glacial origins of rock glaciers (Berthling, 2011).

Under a changing climate, temperatures in the semi-arid to arid Andes are predicted to increase faster and higher compared to their lowlands (Bradley et al., 2006). Concomitant changes in the mountain cryosphere, such as the degradation of glaciers (Braun et al., 2019; Dussaillant et al., 2019), permafrost (Drewes et al., 2018; Rangecroft et al., 2016), and snowpack (Malmros et al., 2018; Saavedra et al., 2018), will strongly affect Andean watersheds currently dominated by runoff

45 generated from snow and ice melt (Barnett et al., 2005; Bradley et al., 2006). Rising air temperatures shift the timing of seasonal snow cover and snow melt resulting in reduced discharges in summer and autumn when demands are highest (Barnett et al., 2005; Bradley et al., 2006). The sensitivity of the Central and Desert Andes of Argentina towards recent warming is reflected by more pronounced snow cover reduction and rising snowline elevations compared to the Western side of the Andes (Saavedra et al., 2018). In the semi-arid Andes of Argentina many active rock glaciers currently exist at or

50 below the zero degree isotherm (Brenning, 2005; Trombotto et al., 1999). In the decades to come, the 0°C isotherm of the mean annual air temperature is predicted to rise more than 500 m under RCP8.5, likely inducing widespread thermal disturbances and permafrost degradation in the Central Andes (Drewes et al., 2018). Generally, ground ice in rock glaciers responds slower to climate change compared to surface snow and ice due to the presence of the seasonally frozen active layer which dampens thermal changes in the subsurface (Haeberli et al., 2006). Massive ground ice and ice-supersaturated,

55 i.e. ice-rich permafrost in rock glaciers are less sensitive to climatic warming than permafrost with low ice content (Scherler et al., 2013) due to complex interactions of advective and convective heat fluxes and latent heat effects during freeze and thaw processes (Scherler et al., 2010). However, ice melt is also predicted for rock glaciers (Marmy et al., 2016) and already observed in the Alps (Mollaret et al., 2019).

In addition, sings of permafrost warming have been reported for many active rock glaciers worldwide, often manifested in
60 rising permafrost temperatures that induce increased surface velocities (Kääb et al., 2007). Borehole data showed that most of the rock glacier deformation occurs within shear horizons of creeping permafrost (Arenson et al., 2002; Haeberli et al., 1998). Velocity variations of rock glaciers are additionally affected by liquid water availability and ground water fluxes (Ikeda et al., 2008) after rain fall and snowmelt indicating increased pore water pressure temporarily enhancing shearing (Cicoira et al., 2019; Kenner et al., 2017; Wirz et al., 2016). Thus, the kinematics of rock glaciers interacts with their

65 hydrology and ground temperatures (Kenner et al., 2019). Interannual vertical variations of the surface topography are mostly related to the mass balance of rock glaciers (Kääb et al., 1998; Konrad et al., 1999), although annual ice gains and losses (Kääb et al., 1997), just as annual water releases as discharge, are significantly lower from rock glaciers than from glaciers (Krainer and Mostler, 2002).

The hydrologic system of rock glaciers receives water from precipitation, snowmelt, ice-melt and groundwater flow, while
70 water is lost by discharge, groundwater flow, evaporation and sublimation (Burger et al., 1999; Krainer et al., 2007). Internal water flow, water storage capacities and changes are controlled by heterogeneous material compositions (debris, ice, water, and air) and their hydrothermal properties (e.g. porosity, solid or liquid phase state of water). On the temporal scale, ice-rich permafrost functions as long-term water storage and aquitard while the active layer functions as short-term reservoir and aquifer (Jones et al., 2018b). Seasonal to annual ice gains and water releases have been mainly attributed to freezing and

75 thawing of the active layer during winter and summer, respectively (Duguay et al., 2015). Rock glaciers can contribute to groundwater recharge and add significant amounts of basin streamflow during late summer, fall and winter (Harrington et al., 2018; Williams et al., 2006). Active layer and permafrost regulate shallow ground water drainage and throughputs as aquifer, aquitard, and/or aquiclude in rock glaciers (Jones et al., 2019). The hydrological response of rock glaciers impacts runoff generation in mountains catchments by delaying and buffering water releases (Geiger et al., 2014; Krainer and

80 Mostler, 2002) depending on the water input and different hydraulic properties of supra-, intra- and sub-permafrost aquifers (Harrington et al., 2018; Jones et al., 2019; Rogger et al., 2017). Moreover, water releases of rock glaciers and permafrost degradation can impact surface freshwater in mountain catchments by changing their inorganic chemistry (Colombo et al., 2018a; Colombo et al., 2018b) and influencing the stream energy budget (Harrington et al., 2017). However, only few

85   studies investigated groundwater flow pathways in rock glaciers (Harrington et al., 2018) and other landforms of mountain watersheds sustaining stream runoff during dry periods (Langston et al., 2011; McClymont et al., 2012; McClymont et al., 2010).

The hydrologic importance of water storage capacities in rock glaciers compared to glaciers (Croce and Milana, 2002; Milana and Maturano, 1999) as well as river discharge (Schrott, 1996) and chemistry during summer months due to the melt of frozen ground (Lecomte et al., 2008) has been previously investigated in the Upper Agua Negra catchment in the dry

90   Andes of Argentina. The present study of the talus rock glacier 'Dos Lenguas' builds upon this earlier research and presents results of high-resolution surface detections and extensive hydro-geophysical subsurface measurements in the data-scarce region of the dry Andes. In-situ electrical resistivity and seismic refraction measurements are combined in an petrophysical model, called four phase model (4PM) (Hauck et al., 2011), in order to quantify the ice and water contents at the end of the thaw season, while imaging the internal hydrologic structure with potential water pathways and ice-rich parts in the rock

95   glacier. Volumetric surface changes are used to infer first order estimations of interannual water storage changes of the active rock glacier.

In spite of speculations on their hydrological significance (Azocar and Brenning, 2010; Corte, 1976; Jones et al., 2018a), almost no quantitative and measurement-based estimates about water storage capacities of Andean rock glaciers and their changes over different time-scales exist. With the present study, we try to fill this gap and aim to: (1) quantify long-term

100 water storage capacities by estimating the current material composition (i.e. the volumetric ice content), (2) analyse surface deformations and gain quantitative estimates of interannual storage changes and (3) infer the internal hydrologic structure of different morphological units of the active rock glacier from the spatial distribution of ice and water contents.

2 Study site

The Upper Agua Negra basin and Dos Lenguas rock glacier are located at approximately 30° S in the dry Andes of

105 Argentina (Fig. 1a). The regional climate is characterised by semi-arid conditions with a mean annual precipitation of roughly 50–150 mm yr^{-1} (TRMM derived estimates (Bookhagen and Burbank, 2006)) and extremely high solar radiation intensities throughout the year (Schrott, 1998). Precipitation above 4000 m asl is mainly solid and falls as snow and sleet during winter. Due to the absent or thin snow cover during eight months of the year, the incoming solar radiation controls surface temperatures and upper ground thermal regime (Schrott, 1991). Few available annual records from different

110 meteorological stations in recent years show mainly negative mean annual air temperature in the catchment (Table 1).

Continuous permafrost has been estimated to cover roughly 16% or 9 km^2 of the watershed above 5200 m asl (Schrott, 1996). The lower limit of discontinuous permafrost has been manifested to reach down to about 4000 m asl potentially covering large areas in the basin, including active rock glaciers (0.88 km^2) (Schrott, 1994; Tapia-Baldis and Trombotto-Liaudat, 2020).

115 Surface ice and snow stored in mountain glaciers (1.4 km^2) and perennial snowfields (0.18 km^2) together account for 2.8% of the watershed (Fig. 1). The high mountain cryosphere of the Upper Agua Negra basin has been one of the areas where previous studies investigated the hydrologic significance of runoff from the high mountain cryosphere. Discharge measurements confirmed that meltwater from areas affected by permafrost conditions and seasonally frozen ground account for an important share of ~20% discharge, which increases up to 30% after snow melt during the ablation season (Schrott,

120 1994; Schrott, 1996). Hydrochemical analysis of melt water indicates significant internal recycling by sublimation and evaporation and delayed meltwater throughputs from rock glaciers (Lecomte et al., 2008). Geophysical investigations on the El Paso rock glacier suggest that the active layer traps and conducts water and interacts with the permafrost table during summer thaw, while ice-rich permafrost is an important water reservoir releasing water mainly during droughts (Croce and Milana, 2002).

125   The Dos Lenguas rock glacier has been the subject of earlier studies (Lecomte et al., 2008; Schrott, 1994; Schrott, 1996). The tongue-shaped talus rock glacier is roughly 1200 m long, between 200 and 600 m wide in its upper and lower part, respectively, and extends from 4200 m at the foot to 4500 m in the root zone (Fig. 1b). Its surface covers an area of ~0.36 km^2 including side and front slopes and 0.25 km^2 excluding them. In its lower part the west-southwest flowing rock glacier separates into a northern and a southern tongue (Dos Lenguas Spanish for "two tongues") both with distinct transverse ridges

130   and furrows terminating in oversteepened frontal slopes (>35°). The surface morphology of the root zone is featured by longitudinal ridges and furrows. In the central part of Dos Lenguas longitudinal ridges transition into transverse structures downslope, where crevasses indicate the splitting of the tongues (Fig. 2). Melt water ponds occur in transversal furrows in the central part and on the northern tongue of Dos Lenguas. The headwall talus system (1.01 km^2) is located at a fault system and delivers mass input to the root zone by rock falls and groundwater from the contributing area above. The debris supply is

135   composed of weathered volcanic rocks of the Permian-Triassic Choiyoi group consisting of rhyolites, dacites, andesites and basaltic lavas, tuffs, breccias and ignimbrites (Heredia et al., 2012; 2002). The rock glacier surface is predominantly characterized by a thin layer (<0.5 m) of coarse pebbles to small boulders supported by a sandy matrix (Schrott, 1994), with isolated large boulders that occur more frequently closer to the headwalls.

3 Methods

140   ### 3.1 Timing of field surveys

All field surveys were carried out between late February and mid-March in 2016, 2017 and 2018. During late summer, the active layer depth and the melt water content could be close their maximum. Therefore, the time span is particularly suitable to detect internal hydrological structures and quantify ice and water contents by means of geophysical methods. The ice content and the liquid water content during the end of the thaw period were only estimated once at each geophysical profile.

145   The horizontal and vertical surface changes were surveyed on a yearly basis with an unmanned aerial vehicle (UAV). Accordingly, interannual storage changes between 2016–17 and 2017–18 were derived from the volumetric changes of the surface towards the end of thaw season.

3.2 DEM generation and analysis

To investigate the kinematics, i.e. vertical and horizontal surface changes, of Dos Lenguas rock glacier, we relied on the

150   production of DEMs from aerial photography collected with an UAV. Using Structure from Motion Multi-View Stereo (SfM-MVS) algorithms, we derived dense point clouds from overlapping aerial imagery with Agisoft Photoscan Professional (Version 1.4.4).

3.2.1 Data acquisition and DEM processing

During late summer in 2016, 2017 and 2018, we surveyed Dos Lenguas using a Phantom 3 Advanced Multicopter equipped

155   with a standard camera (12.4 MP, FOV 94°), taking between 550 and 1800 overlapping images per survey. Survey flights were accomplished in a single day (13/03/2016), or spanning multiple days (24/02 – 02/03/2017 and 03/03 – 07/03/2018), depending on weather conditions. Across the survey area, which covered the rock glacier and its surrounding stable surfaces, we distributed 34 ground control points (Fig. 1b) that were repeatedly measured with a Trimble R8s/R2 differential global navigation satellite system (dGNSS) operating in a real-time kinematic base-rover configuration. The positions of ground

160   control points were recorded with horizontal root-mean-squared errors (RMS) of 0.012 and 0.013 m for 2017 and 2018, respectively and vertical RMS of 0.022 and 0.027 m for 2017 and 2018, respectively. For all three years, the identical workflow was followed in PhotoScan, starting with image alignment, followed by the manual identification of ground control points and camera optimisation.

3.2.2 Measurement of horizontal rock glacier displacement

165   With the advancement of SfM-MVS software solutions and the availability of UAV at low cost, the production of high-resolution DEMs and orthoimages has offered new time-efficient possibilities for the assessment of rock glacier kinematics (Dall'Asta et al., 2017). Here we use two complementary approaches, a) the repeated measurement of 34 ground control points using a dGNSS device and b) an automated image matching approach, to quantify horizontal movement on the rock glacier.

170   For automated image co-registration in optical imagery we used the freely available stand-alone Environmental Motion Tracking (EMT) software (https://tu-dresden.de/geo/emt), originally developed for motion tracking in oblique pictures (Schwalbe and Maas, 2017), but likewise applicable to vertical images. As orthoimages collected in consecutive years show large spectral differences, caused by shadowing effects, snow cover, surface moisture, etc., we used DEMs and their derivatives as input for image matching applications (Dall'Asta et al., 2017). EMT software applies area-based matching to

175   automatically find corresponding patches of pixel values in multi-temporal images using least squares matching or cross-correlation algorithms (Förstner, 1986; Schwalbe and Maas, 2017). Images are loaded into EMT software, where starting points (patch centres) are defined, patch size and search area are set and tracking method as well as master and slave images are selected. While the patch size defines the area of master image values to match, the search area defines the maximum offset of the patch in the slave image. We applied least squares matching with a patch size of 150 x 150 pixel and a search

180   area of 50 x 50 pixel on hillshade images with 0.5 x 0.5 m resolution, resulting in a patch size of 75 x 75 m and a search area of 25 x 25 m.

3.2.3 Volumetric surface changes

Besides analysing the horizontal displacements of the rock glacier, short-term surface elevation changes between two times can be used to approximate the geodetic mass balance of a rock from photogrammetric investigations (Kääb et al., 1998;

185   Kääb et al., 1997) or dGNSS measurements (Konrad et al., 1999).

The production of multi-temporal DEMs allows for the calculation of volumetric surface changes between consecutive surveys. The volumetric changes over the periods 2016–17 and 2017–18 are estimated by subtracting surface elevations of the 2016 DEM from the 2017 DEM and the 2017 DEM from the 2018 DEM, respectively and multiplying by the cell sizes. First order estimates of interannual water storage changes are derived, assuming that the sum of positive and negative

190   volumetric changes which does not equal zero (net balance over one year stated as water equivalent) is mainly caused by melting or gaining ground ice at the transition from the active layer to ice-rich permafrost in the rock glacier. This assumption implies that spatial variations of the flow regime, bulk density changes of debris, and edge effects of surface areas of the rock glacier are included in net balances, but potentially of minor importance for the considered time scale.

Different sources of error might complicate the interpretation of volumetric changes, amongst these errors are dGNSS

195   measurements, manual ground control points tagging, aerial image quality, interpolation algorithm (Wheaton et al., 2010). Therefore, a minimum level of detection (LoD) was calculated that incorporates propagated uncertainties from individual DEMs and determines a threshold to discriminate significant changes from non-significant noise. Following Brasington et al. (2003) we define the minimum LoD using Eq. (1):

$$LoD = t \sqrt{\sigma_{DEM_i}^2 + \sigma_{DEM_{i+1}}^2}, \tag{1}$$

200   where t is the critical value of a given confidence interval in a two-sided student's t-distribution and σ is the standard deviation of the error of the DEM from two epochs. To yield rather conservative estimates of surface changes, we used the root mean square error (RMS) of the individual DEMs as a surrogate for standard deviation (Table 5) and masked out values > –LoD and < LoD for all volumetric calculations.

3.3 Geophysics

205   2-D Electrical resistivity tomography (ERT) and seismic refraction tomography (SRT) were conducted along identical long- and cross-profiles on the Dos Lenguas rock glacier (Fig. 1b) to image the internal structure (Hauck and Kneisel, 2008; Kneisel et al., 2008) and to quantify its material composition based on a petrophysical model, the so-called Four-Phase Model (4PM, see below) (Hauck et al., 2011). Previous studies on the internal structure of rock glaciers have revealed large spatial heterogeneities in material composition within single landforms (Emmert and Kneisel, 2017; Hausmann et al., 2012;
210   Monnier and Kinnard, 2013; Springman et al., 2012).

The layout and survey geometry of the profiles were chosen according to the surface morphology of the rock glacier (Fig. 1b): (i) to gather subsurface properties in the four main structural units of the rock glacier i.e. the root zone (profile C1), the central part (profile C2) and both tongues (profiles L1, L2), (ii) to include longitudinal profiles and cross-profiles, which cover side slopes; (iii) to survey perpendicular to potential water pathways (Langston et al., 2011) and water traps indicated
215   by depressions and local slope of surface topography.

3.3.1 Electrical resistivity tomography (ERT)

Subsurface resistivity is measured by injecting direct current into the ground through two electrodes while measuring the potential difference between two other electrodes coupled to the ground. Iterative tomographic inversions of apparent resistivities measured at different electrode locations and separations along a profile finally yield a two-dimensional model
220   of the specific resistivity of the subsurface. The application of ERT has become a standard technique to image and monitor variations of electrical resistivity in the near subsurface of mountain permafrost due to its sensitivity to the state of water (liquid or solid) in unfrozen and frozen conditions (Hauck, 2013; Hilbich et al., 2008; Mollaret et al., 2019).

Four 2-D ERT profiles were measured with an Abem Terrameter LS system (four channels) with four cables and 81 electrodes. Sponges were placed around steel electrodes and wetted with salt water to reduce contact resistance of the dry
225   and loose surface material (sands and pebbles to boulders) in order to improve galvanic coupling (Maurer and Hauck, 2007). Multiple gradient arrays were measured along all survey lines. Before data inversion, data points exceeding the threshold of 1% of the coefficient of variation have been removed.

Data inversion was done using the Res2Dinv Inversion software (www.geotomosoft.com). Default inversion settings were adapted to comply with high resistivity contrasts on the order of several magnitudes typical for permafrost environments.
230   The robust inversion scheme (L1 norm) with no limits for the resistivity range was used as sharp boundaries and high resistivities for ice-rich permafrost were expected. The mean absolute misfit error of the inversion model is given by the difference between calculated and measured apparent resistivity of the model blocks (Table 2) (Loke, 2018). Data outliers of measured apparent resistivities were filtered using a filter criterion of RMS error >100% after a first inversion run before the inversion was repeated with the filtered data set (Loke, 2018). In total, 92% of all gathered data points were used after
235   filtering (Table 2).

3.3.2 Seismic refraction tomography (SRT)

Similar to the electrical properties, also the elastic properties of the subsurface, measured through its seismic p-wave velocity, are markedly different between frozen and unfrozen state. P-waves are refracted at subsurface layers with velocity contrasts. Subsurface layers and structures can be delineated by analysing first-arrival times at each receiver if velocities
240   increase with depth. Velocity changes in active layer and permafrost are mainly influenced by the porosity of sediments and their saturation with air (330 m s^{-1}), water (1500 m s^{-1}) or ice (3500 m s^{-1}) and are thus more distinct in unconsolidated coarse-grained sediments than consolidated rocks (Hilbich, 2010). P-wave velocities in rock glaciers derived from different field studies increase generally from the active layer (<1500 m s^{-1}) to permafrost (range 1500–5000 m s^{-1}) (Draebing, 2016; Hauck and Kneisel, 2008).

245 Difficulties for the interpretation of structures can arise from overlapping p-wave velocities, e.g. sand (200–2000 m s^{-1}) or bedrock (1300–6200 m s^{-1}, cf. table A.3 in Hauck and Kneisel (2008)) and permafrost in rock glaciers (1500–5000 m s^{-1}, cf. Draebing (2016)). Low-velocity layers sandwiched between or located below high velocities layers cannot be detected from p-waves (Schrott and Hoffmann, 2008). Despite the challenges in mountain permafrost terrain, refraction seismic surveys have been successfully applied on periglacial landforms like rock glaciers (Croce and Milana, 2002; Hausmann et al., 2007;

250 Ikeda, 2006; Musil et al., 2002; Schrott, 1996), moraines (Langston et al., 2011), talus slopes (Otto and Sass, 2006) and debris-covered slopes (Hilbich, 2010)

We used a 24-channel Geode (Geometrics) with 14 Hz Geophones to record seismic waves with a sample interval of 0.125 ms and five stackings per shot point. A sledge hammer (7.5 kg) and an aluminium plate were used to generate p-waves. Eight to ten in-line shots and three to six offset shots were measured for each layout before "rolling" on. The geophone

255 spacing range between 3–5 m according to the spacing of the ERT profiles, as electrode positions were used for geophones to ensure consistent sensor positions within the same geophysical profile (Table 3). The complete data processing workflow, including first arrival picking, travel time analysis and data inversion, was performed with the ReflexW software package that uses an inversion algorithm based on the simultaneous iterative reconstruction technique (Sandmeier, 2016). Profile topography and an initial velocity gradient of 300 m s^{-1}m^{-1} were integrated in all start models. The reliability of the

260 tomograms is given by the RMS and by the sum of the total absolute time differences between observed and calculated travel times (Table 3) (Sandmeier, 2016).

3.2.3 Four-phase-model (4PM)

In order to quantify the material composition of the rock glacier, the complementary ERT and SRT field data were combined in the 4PM to estimate the volumetric fractions of ice, water, air and rock based on petrophysical relationships. Using the

265 ERT-derived inverted specific resistivity distribution ρ and the P-wave velocity distribution from SRT, the 4PM determines the volumetric fractions of liquid water (f_w), ice (f_i), and air (f_a) within the available pore space (or porosity, $\phi = 1 - f_r$, where f_r is the rock fraction) by assuming that the sum of all fractions equals 1 in each model cell of the 2-D model domain (Hauck et al., 2011):

$$f_w + f_i + f_a + f_r = 1 \text{ with } 0 \leq f_w, f_i, f_a, f_r \leq 1 \tag{2}$$

270 In its simplest version, the estimation of f_w in the 4PM is based on Archie's law that relates the measured and inverted electrical resistivity ρ (in Ωm) of sediments to the resistivity of pore water ρ_w, the porosity ϕ and the saturation with water S_w:

$$\rho = a\rho_w\phi^{-m}S_w^{-n} \tag{3}$$

where a (dimensionless factor), m (cementation index) and n (saturation exponent) are empirically determined parameters of

275 the host material (Archie, 1942). This petrophysical relation is assumed to be still valid in partly frozen material and permafrost close to 0°C, where unfrozen water can still be present (Hauck et al., 2011). Regarding the seismic velocities, the 4PM incorporates and extends the time-average equation of Timur (1968) to four phases:

$$\frac{1}{v} = \frac{f_w}{v_w} + \frac{f_r}{v_r} + \frac{f_i}{v_i} + \frac{f_a}{v_a} \tag{4}$$

where v is the obtained p-wave velocity of the bulk material and v_w, v_r, v_i and v_a are p-wave velocities of water, rock, ice

280 and air, respectively (Hauck et al., 2011). Equations (2), (3), and (4) can be combined and solved for f_w, f_i, and f_a by replacing $\phi = 1 - f_r$ and $S_w = f_w / \phi$ in equation (3):

$$f_w = \left(\frac{a\rho_w(1-f_r)^n}{\rho(1-f_r)^m}\right)^{1/n} \tag{5}$$

$$f_i = \frac{v_i v_a}{v_a - v_i}\left[\frac{1}{v} - \frac{f_r}{v_r} - \frac{1-f_r}{v_a} - \left(\frac{a\rho_w(1-f_r)^n}{\rho(1-f_r)^m}\right)^{1/n}\left(\frac{1}{v_w} - \frac{1}{v_a}\right)\right] \tag{6}$$

$$f_a = \frac{v_i v_a}{v_i - v_a} \left[\frac{1}{v} - \frac{f_r}{v_r} - \frac{1-f_r}{v_i} - \left(\frac{a \rho_w (1-f_r)^n}{\rho (1-f_r)^m} \right)^{1/n} \left(\frac{1}{v_w} - \frac{1}{v_i} \right) \right]. \tag{7}$$

285   Thus, Eqs. (5–7) allow to calculate the fractions f_w, f_i, and f_a based on the input data ρ and v and on the used values for the prescribed material properties (ϕ, ρ_w, m, n, v_w, v_r, v_i, and v_a, cf. Table 4). The 4PM has been successfully applied in different mountain permafrost environments (Pellet et al., 2016), including different rock glaciers in the western European Alps (Hauck et al., 2011; Mewes et al., 2017; Schneider et al., 2013). Moreover, the resolution capacity of the 4PM was tested using synthetic models and field data of rock glaciers to assess detectable changes in water and ice content due to

290   permafrost degradation (Mewes et al., 2017).

The most sensitive 4PM parameters from Table 4 are the porosity model ϕ and the pore water resistivity ρ_w (Hauck et al., 2011). Hence, for this study model scenarios with different combinations of ϕ and ρ_w values were performed to estimate and evaluate modelled material compositions. The p-wave velocities v_w, v_r, v_i, v_a and the free parameters in Archie's Law a, m and n were taken from literature (Hauck and Kneisel, 2008; King et al., 1988) and kept constant in the model scenarios.

295   Due to the high spatial variability of grain sizes and ice content in rock glaciers, we used three uniform porosity models with ϕ = 30%, 50%, and 70%, and one mixed porosity model by integrating different porosity ranges of 45–30%, 75–30% and 10–3% for active layer, permafrost and bedrock, respectively (Table 4). The spatial arrangement of mixed porosities was deduced from interpretations of the ERT and SRT data. Negative depth gradients (0.01–0.03 m^{-1}) were included to simulate substrate compaction with depth, while allowing higher ice contents in the upper permafrost. The 30% porosity model is

300   restricted to saturated subsurface conditions, whereas the other models allow supersaturated conditions.

All porosity scenarios were modelled for different pore water resistivities of 30, 50, 100, and 200 Ωm. Modelled pore water resistivities were based on in-situ measurements of specific electrical resistivity of surface waters derived from the spring (~30 Ωm), thermokarst ponds (~50 Ωm), and melted snow from the surface (~ 200 Ωm). A fourth value 100 Ωm was assumed to represent an intermediate model response to snow-derived groundwater increasing its conductivity during

305   percolation.

The 4PM model results were evaluated based on two criteria. First, we used the ratio of the number of model cells with physically consistent solutions (i.e. which satisfied equation (2)), to the total number of model cells as proxy for the suitability of the sensitive 4PM parameters Φ and ρ_w. Second, the model results were qualitatively compared to check plausible material compositions in permafrost and active layer during summer thaw, e.g. whether ice contents in permafrost

310   are sufficient to allow creep deformations and whether model results indicate unreasonable ice contents near the surface, i.e. active layer depths. After the evaluation, plausible conservative and maximum scenarios were chosen in order to estimate ranges of the potential long-term ice content of Dos Lenguas and the liquid water content at the end of the thaw season. The mass of ice and water along the profiles C1 (root zone), C2 (central area), L1 (northern tongue), and L2 (southern tongue) were extrapolated to the surface area of the morphological units (Fig. 1b). The fractions f_i and f_w were converted to mass

315   using densities of 997 kg m^{-3} and 900 kg m^{-3} for water and ice, respectively. The error estimation for the ice and water content in Dos Lenguas was calculated by linearly propagating the uncertainties of (i) mean f_w and mean f_i; (ii) mean model depths; and (iii) two percent attributed to the mapped surface area derived from the high-resolution DEM.

4 Results

4.1 Horizontal surface displacements

320   The Dos Lenguas rock glacier shows a heterogeneous pattern of horizontal surface displacements that are consistent in both direction and magnitude for the two epochs (Fig. 3). Generally, surface velocities fall between a few decimetres and two metres per year and decrease downslope and laterally from the central flowlines towards the side slopes. Highest surface speeds of 1.5–2 m yr^{-1} are attained along the central flowline of the root zone, where surface morphology is dominated by

longitudinal ridges and furrows indicating extensional flow in mainly western direction. Surface movements remain between
1.5–2 m yr^{-1} in the upper central part, while the flow direction slightly turns to west-southwest. Grading into the southern
tongue of the rock glacier, surface displacement decreases only moderately to between 1–1.25 m yr^{-1} and bends towards
southwest. In contrast to this, the boundary between the central part and the northern tongue is much sharper. Here, the flow
continues in west-southwest direction and immediately drops down to below 0.75 m yr^{-1}. Approaching the front of the
northern tongue, surface displacement accelerates again, reaching velocities of up to 1.25 m yr^{-1}. Opposed to this, the
southern tongue further bends towards south-west keeping relatively high surface displacement rates between 1–1.5 m yr^{-1}
before slowing down to 0.75–0.5 m yr^{-1} on top of the frontal slope. Consistently on both frontal slopes, however,
displacement rates rapidly decrease downwards from approximately 1 m yr^{-1} to below the LoD.

The horizontal surface displacement rates confirm the active state of Dos Lenguas, while the displacements of ground
control points with rates smaller than LoD and random bearings (Fig. 3) underline the inactive state of the rock glacier part
north of dos Lenguas classified from surface morphology (Schrott, 1996).

4.2 Volumetric changes

For two epochs, 2016–17 and 2017–18, we calculated vertical surface changes and corresponding volumetric changes for the
five morphological units of the Dos Lenguas rock glacier. The spatial pattern of paired positive and negative annual
volumetric changes of the surface mirrors the downslope deformations of the rock glacier (Fig. 4). The highest amounts of
paired positive and negative changes correlate spatially in the lower central area and along the southern tongue where
strongly developed transverse ridges and furrows match with high horizontal displacements (cf. Figs. 3, 4). Although the
highest displacement rates occurred in the root zone, volumetric changes are less pronounced here, as surface topography is
characterized by longitudinal ridges and furrows. Conversely, weaker volumetric changes occurred also on the northern
tongue, where slower movements of the transverse ridges predominate. At the upper frontal slopes, negative volumetric
changes delineate linear erosion at upper frontal slopes, while positive changes show debris transport and accumulation
further downslope at the lower parts of the frontal slopes of the Northern tongue. Superimposed is a positive volume change
on the upper front slopes, which reflects the advancement and over-steepening of the active rock glacier above the shear
layer, which is also visible at the front slope (cf. Figs. 2a, 3, 4).

If the volumetric changes of the surface topography were produced solely by the interannual forward movement, the sum of
positive and negative volumetric changes, i.e. the net balance, should be close to zero within the given uncertainties.
However, the absolute positive and negative volumetric changes yielded different magnitudes for the total rock glacier
surface (excluding front and side slopes) and the different morphologic units during the observation periods (cf. bar plots in
Fig. 4). Thus, annual net balances of positive and negative volumetric changes, i.e. volumetric gains and losses of ice, were
estimated as a first order estimate of the interannual water storage changes of the active layer given in water equivalents
(Table 5). These interannual storage changes could be also interpreted as mean active layer depth variations above ice-rich
permafrost for the respective surface area and observation period. The volumetric changes of the rock glacier surface
(excluding side and front slopes) signal an annual net balance of –36 mm yr^{-1} and +27 mm yr^{-1} in 2016–17 and 2017–18,
respectively, regarding the 95% confidence interval (Table 5). The spatial differences in the first observation period 2016–17
indicate major ice losses of –61 mm yr^{-1} in the central area and moderate losses between –23 and –30 mm yr^{-1} in the other
morphological units. During the second period 2017–18, the central part, northern tongue, and southern tongue, gained 14
mm yr^{-1}, 45 mm yr^{-1}, and 30 mm yr^{-1}, respectively, while gains of 4 mm yr^{-1} indicate almost equilibrium conditions in the
root zone. Thus, based on the 95% confidence interval, the total net balance between March 2016 and March 2018 indicates
ice losses of –23 mm yr^{-1} and –47 mm yr^{-1} in the root zone and central part, respectively, ice gains of 22 mm yr^{-1} on the
northern tongue, and equilibrium conditions with 0 mm yr^{-1} for the southern tongue.

365   The robustness of volumetric estimates was assessed by calculating LoDs based on different confidence intervals as input to Eq. (1), using *t*-values from a two-sided student's *t*-distribution (Table 5, Fig. 4). Most of the revealed vertical changes from 2016–17 had high limits of detection from 0.232 to 0.576 m for the 70 to 99% confidence intervals, respectively. In contrast, vertical changes from 2017 to 2018 had very narrow limits of detection between 0.073 and 0.183 m for the 70 to 99% confidence intervals, respectively. Thus, even minor surface changes below 0.18 m were detected with high confidences

370   giving high spatial resolutions for the period 2017–18. The LoD 2017–18 is roughly three times smaller than between 2016–17, which might be related to technical difficulties during dGNSS measurements in the 2016 campaign. As a consequence, missing ground control points in the central part of the 2016 DEM likely induced bulging effects causing spatial errors (Mosbrucker et al., 2017) and higher LoDs for 2016–17. Thus, detected volumetric changes between 2017 and 2018 can be regarded as more reliable. However, the 95% and 99% confidence intervals yielded still comparable magnitudes and give

375   rather conservative estimates for both periods.

The derived amounts of interannual storage changes considered as mean depth variations of the active layer indicates potential changes in the range of a few centimetres per year above ice-rich permafrost, even though the detected changes are predominantly related to the ridge and furrow topography. The estimated magnitudes of interannual changes seem reasonable given the high variability of mountain weather conditions, micro-topographic effects, and strong influence of

380   incoming solar radiation potentially controlling local active layer variations on rock glaciers in the Upper Agua Negra catchment (Schrott, 1998). However, the results are first order approximations and uncertainties remain due to assumptions made for the volumetric changes. Nevertheless, positive and negative net balances for this short-term observation period resulted in rather conservative estimates if compared to observed mean annual active layer thickening of >150 mm yr^{-1} at the Morenas Coloradas rock glacier complex in the Central Andes of Mendoza between 1992 and 2007 (Trombotto and

385   Borzotta, 2009).

4.3 Internal structure, ice and water contents

4.3.1 ERT results and interpretations

The inversion results of all ERT data show a heterogeneous distribution of high, intermediate and low specific resistivities the rock glacier (Fig. 5). High resistivity zones (> 10^4 Ω m) are mainly located underneath ridges of the rock glacier reaching

390   depths of 10–30 m below the surface. Low resistivities (< 10^3 Ω m) predominantly occur in and near topographic depressions close to the surface in all profiles or below high resistivities at depths of approximately 40 m in both cross-profiles (C1 and C2) and below depths of 35 m in the longitudinal profile L2 (Fig. 5)

According to the heterogeneous pattern of resistivity ranges as well as field observations of the surface debris along the profiles, the resistivity ranges were interpreted to be invoked by variable active layer and permafrost conditions: (i) Low

395   electrical resistivities (< 10^3) Ωm correspond to unfrozen and wet subsurface conditions; (ii) High electrical resistivities (> 10^4 Ωm) close to the surface show dry unconfined sands and/or coarser debris with large voids, while high electrical resistivities (>10^4 Ωm) in the subsurface indicate rather ice-rich permafrost in the rock glacier. Thus, it has to be noted that the delineated structures of active layer and permafrost might be invoked by various substrate characteristics (lithology, grain sizes, porosities), different fillings of voids by ice, water and air and the subsurface temperature regime. Yet, the

400   interpreted structures indicate that active layer is mainly characterised by very dry debris of ridges and locally wet conditions located in longitudinal and compressional furrows or in topographic depression between side slopes and talus slopes of the rock glacier (Fig. 5). Direct proof of wet active layer conditions is given at L1 where melt water ponds are present in furrows next to the profile (Fig. 2d) on the northern tongue. However, horizontal and vertical contrasts and anomalies of resistivity did permit a clear delimitation of the permafrost body in the rock glacier. Resistivities from 10^3 and 10^4 Ωm below

405   depressions and furrows could indicate higher water and/or lower ice content in the rock glacier due to percolating water and/or local permafrost degradation between interpreted ice-rich permafrost (>10^4 Ωm). Ice-rich permafrost shows large

vertical variations and increasing thicknesses of 10–20 m, 15–25 m, and 15–30 m in the root zone, central area and both tongues, respectively. As the electrical conductivity (=1/resistivity) is mostly sensitive to liquid water content, it remains inconclusive if higher resistivities may be are caused by air or ice filled voids. Additionally, inversion model sensitivity

410 decreases with depth and towards lateral borders of the ERT, and high resistivity contrasts can cause inversion artefacts in the model (Hilbich et al., 2009; Marescot et al., 2003). Nevertheless, the mean thickness of ice-rich permafrost was roughly approximated from the vertical dimensions of high resistivities zones 15±5 m, 20±5 m and 22±7 m in the root zone, central area and both tongues, respectively (cf. interpreted structures in Fig 5).

4.3.2 SRT results and interpretations

415 All SRT profiles reveal a horizontal two layer structure of smoothly increasing p-wave velocities with depth (Fig. 6). P-wave velocities <600 m s^{-1} of the active layer reflect dry unconfined sands and pebble to boulder sized material close to the surface (<3 m depth). Increasing velocities up to 1500 m s^{-1} at depths of 3–8 m indicate a more compacted and/or moister sandy material above the permafrost table. Inverted p-wave velocities of the lower layer have a wide range from 1500–5000 m s^{-1} thereby showing spatially heterogeneous velocity distributions. The upper low velocity layer (<1500 m s^{-1}) was

420 interpreted to represent unfrozen areas, while the intermediate to high velocity layer (1500–4500 m s^{-1}) indicates permafrost. The gradually increasing p-wave velocities are partly vertically incised between higher p-wave velocities (cf. 2000 m s^{-1} isoline in Fig. 6) indicating a transition from unfrozen debris to permafrost between 1500–2000 m s^{-1} during summer thaw which has been observed on previous seismic surveys of rock glaciers in the study area (Croce and Milana, 2002; Schrott, 1994). The p-wave velocities of the transition area could either indicate the presence of water ($v_w = 1500$ m s^{-1}) and lower

425 ice content and/or be related to the vertical resolution of the smoothly inverted p-wave velocities.

Higher velocities indicate ice-rich permafrost (2500–4500 m s^{-1}) and bedrock occurrences (> 4500 m s^{-1}), where Dos Lenguas starts to split up (cf. Figs. 6b, 6c) and below the talus slope next to the root area (cf. Fig. 6a). However, a reliable discrimination between frozen unconsolidated rocks, and bedrock is difficult due to the large overlapping p-wave velocity ranges of permafrost (Draebing, 2016; Schrott and Hoffmann, 2008), and volcanic rocks (Schön, 2011), and the limited

430 resolution capacity in the lowest parts of the models.

Comparing the velocity patterns to resistivity distributions show similar vertical structures and anomalies, e.g. along cross-profile C2 between 150 and 200 m (cf. Fig. 5b, 6b) where open crevasses expose fine material due to the rupturing of Dos Lenguas (Fig. 2b). However, large variations of active layer depth could be interpreted due to heterogeneous patterns observed in ERT and SRT. Yet, both methods locally indicate the influence of water in unfrozen areas potentially affecting

435 permafrost composition underneath. Interpreted bedrock structures from SRT were transferred to the mixed porosity model of the 4PM. The combined interpretation of ERT and SRT data is given in the following section.

4.3.3 4PM results and interpretations

The 4PM was applied to quantify the ice and water content of Dos Lenguas based on complementary ERT and SRT measurements. The spatial distribution of the ice and water contents can then be used to estimate the internal hydrological

440 structure of the rock glacier. In general, the 4PM results show the heterogeneous material composition in the rock glacier (Figs. 7, 8).

Along all profiles, modelled mean fractions of ice (f_i) and water (f_w) of all scenarios show increasing ice content with higher porositiy and increasing water content with higher pore water resistivity, respectivly (Fig. 7). Modelled mean f_w over the full model depth show local maxima, where reduced ice contents occur along the profiles. Mean f_i range roughly from 5 to 15%,

445 20 to 30%, and 40 to 50% for the uniform porosity models with 30%, 50%, and 70%, respectively. The mixed porosity model yielded intermediate mean f_i values that range between the uniform 50% and 70% porosity models. The porosity

variations of ice-rich permafrost and bedrock structures that were found within the interpreted ERT and SRT profiles were built into this "best guess" mixed porosity model.

The 4PM scenarios using the highest porosities and lowest pore water resistivities yielded the highest quantities of physically
450 consistent numerical solutions, whereas scenarios with lower porosities and higher pore water resistivities yielded the lowest quantities of physically consistent numerical solutions (Table 6). Thus along all profiles, the scenario using $\phi_{uniform} = 70\%$ and $\rho_w = 30\ \Omega m$ yielded the highest amount of physical consistent model solutions giving the highest volumetric ice contents and lowest mean fraction of water. However, despite resulting in maximal physically consistent model solutions for all profiles, the respective model results showed substantial ice contents within the active layer close to the surface, which is
455 clearly unrealistic. Hence, the model scenario using variable porosities for active layer, permafrost and bedrock were interpreted as most plausible. This mixed porosity model provided conservative estimates for f_i, since these scenarios prevent overestimations caused by uniform porosity assumptions. Likewise, pore water resistivities of $30\ \Omega m$ and $50\ \Omega m$ were interpreted as most plausible, as the scenarios using higher pore water resistivities reduced the ice content, while the modelled water content in active layer and permafrost were unreasonable high for the dry mountain environment. Thus,
460 lower solved model cell ratios, relative low mean ice contents ($< 40\%$), and unreasonable high water contents of the 4PM scenarios with $\phi \leq 50\%$ and $\rho_w \geq 100\ \Omega m$ were interpreted as not suitable and less plausible for an active rock glacier with displacement rates up to 2 m yr^{-1}. Consequently, the scenario with $\phi_{uniform} = 70\%$ and $\rho_w = 30\ \Omega m$ was interpreted as maximum model for the ice content estimation, while the scenario with ϕ_{mixed} and $\rho_w = 50\ \Omega m$ represents conservative ice content estimates along the profiles. Based on these scenarios, the calculated mass of ice and water in the rock glacier
465 ranges from 1.71×10^9 kg ($\pm42\%$) to 2.00×10^9 kg ($\pm44\%$) and from 0.36×10^9 kg ($\pm32\%$) to 0.43×10^9 kg ($\pm32\%$), respectively (Table 6).

The modelled fractions of ice and water content per porosity were used to infer the internal hydrological structure of Dos Lenguas towards the end of the thaw season (Fig. 8), as they indicate the spatial distribution of active layer, ice-rich permafrost, and areas influenced by shallow groundwater pathways and storages for the scenario with ϕ_{mixed} and $\rho_w = 50$
470 Ωm (figures of all modelled scenarios are shown in the supplements (S1)). Ice-free model cells indicate the active layer depth above model cells containing ice. Ice saturation per porosity varies spatially strongly from ~30% to 90%. Modelled ice-rich permafrost is dissected by permafrost conditions with lower ice saturations (<40%). Water saturations >10% show locations with moist to saturated conditions that occur preferentially beneath and close to depressions of longitudinal and transvers furrows. Water saturations <10% indicate either relatively dry conditions of the active layer close to the surface or
475 minor amounts of liquid water in permafrost. A high water saturation indicates potential water pathways and traps in the rock glacier during summer thaw in potentially unfrozen areas (no ice content) and were interpreted to function as seasonal aquifers. Where increased water content and reduced ice content overlap underneath wet active layer conditions, the model results suggest the infiltration of water and/or presence of water pathways and traps between ice-rich permafrost (e.g. at ~160 m in profile C1, Fig.8a). Therefore, intra-permafrost flow could occur locally and rock glacier permafrost could locally
480 function as aquitard in the thaw season.

The spatial occurrence of increased ground water contents and the visible thermokarst ponds indicate a strong influence of the ridge and furrow topography on the water pathways and traps within the rock glacier (cf. Figs. 8, 9). The water content distribution of profile C1 in the root zone indicates the presence of water pathways below longitudinal furrows and aquifers from adjacent talus slopes. Profile C2 indicates water pathways in the active layer and below the northern side slope, and
485 sub-permafrost or intra-permafrost aquifers where bedrock porosities have been implemented. Vertical structures with increased water and reduced ice saturations could indicate water pathways along crevasses in the central part of the profile, where Dos Lenguas starts to split up. The longitudinal profile L1 on the northern tongue shows water pathways and traps below compressional furrows and indicates a bedrock aquifer below ice-rich permafrost. Melt water ponds next to L1 (Fig. 2) are consistent with modelled shallow ground water content in the depressions. Profile L2 on the southern tongue indicates

490   aquifers between compressional ridges in the active layer and an aquitard between ice-rich permafrost. More details on the
         internal hydrological structure are discussed below in combination with interannual surface changes of the rock glacier.

5 Discussion

5.1 Methodological discussion

5.1.1 Volumetric changes

495   The sum of positive and negative volumetric changes of the rock glacier surface gives a first order estimate of interannual
         water storage changes due to seasonal freeze and thaw processes in the subsurface. However, our results do not show a clear
         signal of positive and negative interannual changes in different morphological units of Dos Lenguas over the two-year
         observation period (Fig. 10b). Although the interannual net changes are dominated by ice gains and losses in the subsurface
         (Kääb et al., 1998), vertical surface changes are additionally caused by three dimensional creep deformations, accumulation
500   and excavations, and compression and consolidation of the sediments (Kääb et al., 1997).
         Our volumetric estimates exclude values that lie within the LoDs of respective confidence intervals, translating to cut-off
         limits of ±0.368 m and ±0.117 m for the 90% confidence interval for 2016–17 and 2017–18, respectively (Table 5).
         Assuming incompressibility of the Gruben rock glacier, vertical changes associated with the spatial variations of the flow
         regime have been estimated to attain magnitudes on the order of cm yr^{-1} (Kääb et al., 1998). Similarly, Konrad et al. (1999)
505   estimated that vertical changes from differential ice gains and losses of the Galena Greek rock glacier are one order of
         magnitude greater than vertical changes induced by the flux of ice, assuming isotropic creep behaviour, ice thickness and no
         basal sliding of the rock glacier. Thus, our calculated interannual vertical changes based on LoDs are at least one magnitude
         greater than vertical changes expected from spatial variations of the flow regime. We are therefore confident, that net
         balances derived from volumetric surface changes reliably estimate interannual storages changes dominantly associated with
510   ice gains and losses, though these might well incorporate minor contributions from three-dimensional creep deformations
         and/or changes in bulk densities of the rock glacier material.

5.1.2 Geophysical approach

         The 4PM approach was applied for a first quantitative approximation of the water and ice content of the active talus rock
         glacier Dos Lenguas in the semi-arid Andes of Argentina. In the absence of a-priori information or calibration data from
515   boreholes for the 4PM (Pellet et al., 2016), the most sensitive model parameters Φ and ρ_w were used to build scenarios to
         cover a plausible range of model estimations and to account for uncertainties arising from the heterogeneous material
         composition observed in drill cores of rock glaciers (Arenson et al., 2002). In combination with the large spatial coverage of
         the conducted 2-D geophysical surveys, this approach is considered to yield plausible ranges of ice and water contents for
         the whole rock glacier. Previous studies applying and testing the 4PM on rock glaciers showed that estimated ice and water
520   contents can be reasonable well delineated and are in good agreement with nearby boreholes and complementary data sets
         (Hauck et al., 2011; Mewes et al., 2017; Schneider et al., 2013).
         However, several limitations accompanied the geophysical approach, which are mainly caused by the inherent ambiguity of
         ERT and SRT inversion and the uncertainties associated with the petrophysical relationships, and their free parameters, used
         in the 4PM (Duvillard et al., 2018; Hauck et al., 2011; Mewes et al., 2017). In addition, the spatial resolution of the
525   geophysical approach depends on the sensor spacing in the field in relation to the dimension of the observed layers and
         anomalies causing a trade-off between the spatial coverage of the landform (profile length and investigation depth) and the
         resolution capacity for small scale structures in the model domain. Mewes et al. (2017) showed that the resolution capacity
         of the 4PM is suitable to detect hydrological structures and permafrost degradation in rock glaciers with sensor spacings
         comparable to the spacings used in this study (Tables 2, 3). However they empasize that the resolution capacity of vertical

530   structures is generally good in the 4PM, whereas horizontal saturated layers may be overestimated due to inversion artefacts
(Mewes et al., 2017).

With respect to the SRT input data, the accuracy or data misfit between our modelled and observed travel times of roughly 2
ms (Table 3) is in good accordance with SRT results from other permafrost investigations (Hilbich, 2010; Krautblatter and
Draebing, 2014). However, modelled p-wave velocities towards the base of the tomograms have lower confidences (Hilbich,

535   2010) due to generally decreasing ray densities with increasing depth that limit the interpretations of overlapping velocity
ranges (Draebing, 2016; Schrott and Hoffmann, 2008) in deepest model areas.

The overall quality of ERT data is very good considering the extreme rock glacier conditions, with mean absolute misfit
errors of the inversion models between 5.1 and 7.4% and only 7.7% filtered data points during processing (Table 2). We
used the multiple gradient measurement as input for the 4PM as this configuration yields a higher spatial resolution of

540   horizontal and vertical resistivity heterogeneities in the inversion models (Aizebeokhai and Oyeyemi, 2014) compared to the
Wenner array (Dahlin and Zhou, 2004). Nevertheless, higher uncertainties remain in and below high resistive ice-rich
permafrost (Hilbich et al., 2009) and towards lateral and lower boundaries of ERT profiles due to the low sensitivities in
these model areas.

Vertical dimensions of saturated horizontal aquifers above the permafrost body can be overestimated in the 4PM due to

545   inversion artefacts of ERT as demonstrated in Mewes et al. (2017). As a consequence, the thickness of the 4PM-derived
aquifers (Fig. 8) and calculated water contents close to the surface could be overestimated where large resistivity contrasts
(Fig. 5) occur while in turn ice contents might be underestimated in these model parts. However, almost saturated aquifer
conditions (~70% $f_w \, \Phi^{-1}$) close to the surface were only modelled at profile L2, where a thermokarst pond in the furrow next
to the profile confirms saturated active layer conditions (cf. Figs. 2, 9). Besides that, only potential bedrock occurrences with

550   low porosities indicate saturated conditions. Although theses saturated aquifers could be overestimated in their vertical
dimension (Fig. 8), all other interpreted aquifers and aquitards indicate unsaturated conditions with lower fractions of water
contents per porosity of <50% or <20%, respectively. Concomitant with these moist conditions at the transition from active
layer to permafrost, observed p-wave velocity patterns indicate relatively low permafrost velocities of 1500–2000 m s^{-1} (Fig.
6). This range of p-wave velocities correlates well with decreasing p-wave velocities of permafrost from austral summer to

555   autumn ranging between 1500 and 2400 m s^{-1} compared to 3400 m s^{-1} during winter found at the neighbouring El Paso rock
glacier (Croce and Milana, 2002). Thus, relatively low inverted velocities <2000 m s^{-1} may potentially indicate the seasonal
influences of permafrost thaw and increased melt water contents at the permafrost table.

5.2 Spatial pattern and interrelations of internal hydrologic structures and surface kinematics

In order to interrelate spatial heterogeneities of internal hydrological structures of the rock glacier during summer thaw we

560   now focus on the individual morphologic units and the concurrent observed vertical and horizontal surface velocities.

5.2.1 Root zone

Cross-profile C1 reveals the influence of shallow ground water on the ice content and the internal hydrologic structure of the
root zone of the rock glacier (Fig. 8a). The 4PM results suggest that the central longitudinal depression at the surface of the
rock glacier (horizontal distance 150 m) acts as a trap and pathway for ground and melt water from the contributing area

565   above. Here, the relatively high water contents in the active layer are in accordance with observed wet surface debris a few
hours before the field measurements due to previous precipitation and snow melt. While the rock glacier composition below
this depression is characterized by reduced ice and elevated water contents, areas below longitudinal ridges show ice-rich
permafrost. This suggested interplay of reduced ice contents and increased water content could be related to different
processes: First, the highest surface velocities of 1.5–2 m yr^{-1} occur along the central flow line characterizing an extensional

570   flow regime with longitudinal furrows (Fig. 10). The extensional deformation potentially creates drainage pathways for melt

and shallow groundwater from the active layer that infiltrates into the ground ice of the rock glacier (Ikeda et al., 2008), increasing the hydraulic conductivity of ice-rich permafrost and shifting the rock glacier body from an aquiclude towards an aquitard (Fig. 8, 10). Second, increased water contents could be related to local permafrost degradation, seasonal thawing or talik evolution due to localised effects of either conduction, radiation or advection effects of water or air (Haeberli et al.,

575 2006; Luethi et al., 2017; Scherler et al., 2013). Negative and positive vertical changes in the root zone show a spatially heterogeneous pattern with ice gains and losses in 2016–17 and in 2017–18, respectively (Fig.10). Therefore, homogeneous thaw settlement can be excluded from our data over the observation period 2016–2018 (Fig.4) and it is more likely that locally increased water contents point to water pathways below longitudinal furrows and/or seasonal thaw effects induced by the micro-topography (Fig. 10). Besides internally developed water pathways in active layer and permafrost, subsurface

580 compositions of adjacent side slopes illustrate the influence of ground water draining towards a sub-permafrost aquifer from the side and talus slopes below the root zone of Dos Lenguas (horizontal distances < 50 and > 250 in Fig. 8a). The Northern left part of the profile shows little ice remnants and shallow ground water influences of the talus slope from the inactive rock glacier next to Dos Lenguas, while the lower parts of the southern talus slope depicts water saturated conditions for assumed bedrock porosities in the 4PM.

585 The generally high horizontal velocities > 1 m yr^{-1} in the root zone compared to the other morphological units could be related to ice-rich permafrost above bedrock, steepest mean slopes of the surface, and might be enhanced by increased water supply from the surface and catchment, which reduces resisting forces in shear layers due to positive pore water pressures (Kenner et al., 2017).

5.2.2 Central part

590 The influence of groundwater draining underneath the active rock glacier from the northern depression at the side slope is also suggested in the cross-profile C2 (Fig. 8b). High seismic velocities at 20 to 30 m depth below the surface indicate bedrock occurrences in the lower central part of the rock glacier that were incorporated in the mixed porosity model of the 4PM, which indicates an unfrozen and water saturated bedrock aquifer. The permafrost body above bedrock shows vertical structures with increased water and reduced ice contents illustrating water pathways along filled fissures and crevasses in the

595 subsurface due to the splitting of the central rock glacier part into the northern and southern tongues (see also vertical structures of ERT and SRT in Fig. 5b and Fig. 6b, respectively). Locally, relatively high water contents could indicate channelized unsaturated aquifers in the southern part of the profile.

The spatial pattern of horizontal surface velocities generally shows a decelerating trend approaching the tongues (Fig. 3), portraying the transition from extensional to compressional flow that is also expressed in a transition from longitudinal

600 structures to transverse ridge and furrow topography. Further downslope, the moving rock glacier mass decelerates towards the less inclined northern tongue, while the surface velocities remain high in direction of the southern tongue. As a consequence, lateral velocity contrasts of ~0.5 m yr^{-1} cause shear-induced tearing apart of the tongues in the lower central part of Dos Lenguas, which is also documented by longitudinal rupturing of transverse ridges with open crevasses at the surface (Fig. 2). These surface findings are corroborated by higher mean air contents at C2 compared to C1 (cf. Table 6 and

605 supplements S1) indicating a thickening of the active layer and a lateral spread of the cross-section from the root zone towards the lower central part.

The volumetric changes of 2017–18 are increased in the central part (14 mm yr^{-1}) compared to the root zone (1 mm yr^{-1}). The spatial pattern of gains and losses illustrates higher volumetric changes along distinct transverse ridges and furrows in the lower part of the central area. Besides mimicking the advance of ridges and furrows (Kääb et al., 2003; Kääb and Weber,

610 2004), the small scale topography might enhance differential ice gain and losses (Kääb et al., 1998) due to shading effects in furrows preventing direct sublimation of snow and vaporisation of water. Thus, meltwater infiltration could be more efficient in furrows due to micro-topographic effects. In addition, shallow groundwater drainage along furrows (4PM) could be

transferred to lower rock glacier areas and locally be trapped in the deepest parts of transverse furrows. This process is indicated by potential aquifers and drainage pathways along furrows in C1 and C2 and a thermokarst pond with a delta in the central part (Fig. 2), as well as water traps in transverse furrows of both tongues (cf. Figs. 8, 9, 10).

5.2.3 Tongues

Below the Northern tongue our results indicate an extended bedrock occurrence from the central part further downslope. Ice-rich permafrost is dissected by areas with high water contents, indicating aquifers and water drainage along furrows (cf. Figs. 8, 9). Here, 4PM results are in accordance with direct observations of thermokarst ponds occurring 20–30 m south of the profile, where meltwater is trapped and exposed at the surface in the deepest part of the furrows. This is similar to L2 on the southern tongue, where high water contents indicate unsaturated aquifers and water traps located in depressions in front of and behind of compressional ridges. Moreover, gully like structures on the surface perpendicular to transvers ridges and furrows indicate thermal erosion along meltwater pathways in the subsurface in some parts of the southern tongues (cf. Figs. 2, 8, 9).

The flatter northern tongue, hosting numerous thermokarst ponds, shows the largest positive interannual storage change 2017–18 and is the only morphological unit of Dos Lenguas, which gained ice over both observation years. The steeper southern tongue appeared to be in equilibrium between 2016 and 2018 with equal negative and positive interannual storage changes of 30 mm yr^{-1} in 2016–17 and 2017–18, respectively (Fig. 10). The increasing interannual storage changes from the root zone over the central parts to both tongues in 2017–18 could reflect the role of drainage pathways and water traps in and along furrows. Longitudinal furrows could build more effective drainage pathways transferring meltwater inputs downslope from steeper areas of the rock glacier. Decreasing mean surface slopes and a strong transverse ridge and furrow topography might better trap and collect inputs from drainage pathways and percolating water from the surface (precipitation, snow melt). On both tongues, shallow aquifers and meltwater traps along transverse furrows (Figs. 9, 10) overlap with the spatial pattern of locally increased volume gains and losses. Especially along transverse ridges and furrows with increased water contents, meltwater and ground ice could interact at the permafrost table, potentially causing significant amounts of volumetric changes and respective vertical changes due to the seasonal thaw of an ice-rich permafrost table and/or refreezing of a wet active layer bottom.

The clear contrast in horizontal velocities between both tongues coincides with the overall slope gradient. While the steeply descending southern tongue experiences high horizontal velocities of 0.75–1.5 m yr^{-1}, potentially enhanced by the influence of melt water, the generally flatter northern tongue, shows decelerated horizontal surface velocities (0.25–1.0 m yr^{-1}), potentially also related to bedrock obstacles at the rock glacier bed. Whereas the southern tongue decelerates towards its front, the surface velocities of the Northern tongue accelerate towards the steep frontal slope mimicking the creep behaviour of over-steepened cliffs (Cuffey and Paterson, 2010).

5.2.4 Front and side slopes

Surface velocities generally decrease towards the side and frontal slopes given the increase in friction, which indicates lower or no ice content within material accumulated at the outer margins. Lower to no ice contents within the side slopes is also indicated in the 4PM derived material composition of the cross-profiles C1 and C2.

The advancement of the rock glacier is reflected by volumetric changes and horizontal displacement at the front slopes. Here, two superimposed processes act: First, the upper front is over-steepened (>35°) by permafrost creep, and second, gravitational processes transfer debris to lower front slope positions. The over-steepened advance of the upper slope shows increasing horizontal displacement rates towards the surface, indicating cumulative deformations of creeping permafrost. From digital topography we further delineate the approximate depth of the shear horizon and the stiff basal layer below (Figs. 2, 9). Derived depths of 20–25 m and 15–20 m at the northern and southern tongue, respectively, match roughly to

observed depth ranges of ice-rich permafrost in ERT and 4PM profiles. Whether the stiff basal layer below the shear horizon and deeper parts of the rock glacier are frozen or unfrozen, potentially functioning as sub-permafrost aquifer (Haeberli et al., 1998), or intra-permafrost aquifers in case of talik evolution (Kenner et al., 2017; Luethi et al., 2017), remains unclear judging from our data. However, our detected depths of ice-rich permafrost and calculated ice and water contents in Dos Lenguas are in line with borehole data from active rock glaciers in the Alps which revealed that ice-rich permafrost and internal deformations occur mainly in and above shear zones in depths of less than ~30 m (Arenson et al., 2002; Buchli et al., 2018; Haeberli et al., 1998; Kenner et al., 2017; Krainer et al., 2017). As a consequence, estimations of ice contents in active rock glaciers should exclude side and front slopes and the depth of ice-rich permafrost should be either limited (threshold <30 m depth) or based on observations. Taking this into account could in particular improve potential estimates of regional water storage capacities of rock glaciers that were based on area thickness relationships (Azocar and Brenning, 2010; Jones et al., 2018a; Rangecroft et al., 2015) in order to avoid overestimations of ice-rich permafrost thicknesses in large rock glaciers.

Frontal advances by accumulated sediment at the frontal slopes revealed that Dos Lenguas efficiently transports sediments, deposits and overruns them. Long-term sediment transfer and slope instabilities at the front of the northern tongue (Kummert et al., 2018) could further push the Agua Negra river towards the opposite valley side, putting the pass route at risk and/or building a rock glacier dam that endangers downstream infrastructures and modulates sediment and water transfer (Blöthe et al., 2019).

5.3 Water storage capacities and interannual changes

In the following we interrelate water and ice storage capacities and the interannual changes for the active rock glacier. The overall long-term ice storage of this rock glacier ranges between $1.71–2 \times 10^9$ kg according to the most reasonable 4PM scenarios (Table 6). The liquid water content towards the end of the thaw season was $0.36–0.43 \times 10^9$ kg (Table 6) corresponding to 21–22% of the long-term ice storage and 17–18% of overall liquid water and ice content of the rock glacier. Due to the uncertainties in quantifying thin water layers from ERT data mentioned above, this estimate must be seen as an upper bound. Thus, roughly a maximum of one fifth of the total water storage capacities could be involved in water exchange and transfer during thaw season based on the material compositions of Dos Lenguas.

Interannual storage changes derived from volumetric changes at the surface revealed that only 3–6% of the total liquid water content was lost between austral summers 2016 and 2017 or gained between 2017 and 2018 according to the 95% confidence interval with -36 mm a^{-1} (-19.8×10^6 kg) and 28 mm a^{-1} (14.7×10^6 kg), respectively. Nevertheless, the given amounts of interannual storage changes suggest that a significant share of annual precipitation can be stored in and released from the active rock glacier in this part of the dry Andes that receives annual precipitation rates between 50–150 mm yr^{-1} (TRMM derived estimates (Bookhagen and Burbank, 2006)). The interannual storage changes of the active rock glacier could be influenced by the high variability of mountain weather conditions throughout the year in the semi-arid catchment. The MAAT $< 0°$ C at the altitudinal range of Dos Lenguas from 2015–2019 generally point to permafrost conditions. Recorded ground surface temperature of Dos Lenguas during the observation period 2016–2018 (Fig. S17) indicate that the highly variable temperature regime influences the negative and positive interannual storage changes of Dos Lenguas in 2016–17 and 2017–18, respectively due to an earlier onset, as well as a delayed and higher summer maximum during the ablation period 2016–17 compared to 2017–18.

The constant discharge of 5–8 l s^{-1} from the Dos Lenguas spring found by Schrott (1996) would translate to a total of 64.8–103.7×10^6 kg for a five month lasting thaw season. Comparing the potential total discharge at the spring with the total liquid water content in late summers indicates that only 14–30% of the seasonal groundwater could be transferred to the Agua Negra river, while 70–86% of groundwater could be involved in refilling and exchanging ground water storages and aquifers in and below the rock glacier. Therefore, the estimated ice and water storage capacities and the interannual storage

changes demonstrate that an active rock glacier like Dos Lenguas could play a crucial role in buffering and regulating seasonal groundwater flow and recharge, while constituting a long-term ice storage in the dry high mountain catchment, where currently only 2.8% of the surface area remain permanently covered with surface ice and snow.

Given the widespread distribution (IANIGLA, 2018) and the slower response of active rock glaciers (Haeberli et al., 2006) to the predicted temperature increases in the dry Andes (Barnett et al., 2005) compared to down-wasting Andean glaciers (Braun et al., 2019) suggests that long-term water storages and seasonal buffers in ice-rich permafrost and active layer, respectively could become more important for Andean watersheds.

6 Conclusions

Water storage capacities and interannual changes were quantified for an active rock glacier in the semi-arid Andes of Argentina. For this, we interrelated surface changes and the material composition in different morphological units of the Dos Lenguas rock glacier. Based on digital elevation models and their derivatives from Structure from Motion Multi-View Stereo algorithms, horizontal and volumetric surface changes were calculated using motion tracking and Digital Elevation Models of Difference, respectively. Electrical resistivity and seismic refraction tomography data sets from field measurements were used as input data for a petrophysical model. Ice and water contents were quantified based on different scenarios of the most sensitive parameters used in the 4PM. Additionally, spatial heterogeneities of ice and water contents revealed the internal hydrological structure of Dos Lenguas towards the end of the thaw season.

Increased water contents in depressions and furrows, and ice-rich permafrost below ridges indicate interactions of the distinct ridge and furrow topography and material composition in the subsurface of Dos Lenguas rock glacier. The geophysics-derived aquifers in seasonal unfrozen ground, taliks and potential aquitards through thawing ice- rich permafrost function as water traps and pathways during the thaw period, while the observed ground ice occurrences are structuring the internal hydrology of the rock glacier. Net balances derived from volumetric surface changes for 2016–17 and 2017–18 give first order estimates of interannual water storage changes of the active rock glacier Dos Lenguas.

Our findings suggest that water storage capacities and interannual storage changes can be estimated using interrelations from surface and subsurface properties, despite the uncertainties arising from the spatial heterogeneities and indirect measurements. We conclude that the ice content and interannual storage changes of the active rock glacier Dos Lenguas represent an important long-term water reservoir and buffer in addition to other rock glaciers and ice-rich permafrost occurrences in the Upper Negra catchment, as less than 3% of the dry mountain catchment is covered with surface ice. The interannual storage changes suggest that a significant portion of annual precipitation can be buffered and/or released by seasonal ground freeze and thaw processes in active rock glaciers of dry mountain catchments. The detection of basal layers at rock glacier fronts may help to better constrain depths and volumes of ice-rich permafrost for different rock glacier types and sizes and could further help to calibrate area thickness relationships. Front and side slopes should be excluded from rock glacier areas to avoid overestimations of local, and especially, regional water storage estimations. This study closes an important knowledge gap with respect to the quantification of ice contents and water storages changes of rock glaciers in the dry Andes and can serve as a benchmark for regional ice/water estimations using rock glacier inventories.

For further understandings of rock glacier hydrology, such field-based studies and monitoring approaches are necessary to elucidate quantities and functions of long- and short-term storage changes, as well as their interactions with catchment hydrology. Especially in dry mountain catchments further insights into hydrological contributions, functions, and changes in active rock glaciers might become more important under climate change forcing rapid adaptions in the cryosphere.

Data availability. The data sets can be obtained on request to the authors.

Supplement. The supplement related to this article is available online.

Author contributions. CH designed the study, conducted field work, collected and processed geophysical and SfM data,
740   wrote manuscript and conceptualized figures; JB collected and processed SfM data, helped with data processing, conducted
field work; CTB and DT contributed to field logistics and data acquisition; CHi and CHa helped with geophysical data
processing and analysis; LS conducted field work, contributed to study design, data acquisition, obtained funding; all authors
contributed to the revision of the text.

745   **Acknowledgements**

This research was funded by the German Research Foundation (SCHR 648/3-1). We further thank Lorenz Banzer, Henning
Clemens, Nico Griesang, Friedrich Fröhlich, Gerrit Heinmüller, Thorsten Höser, Julius Isigkeit, Martin Mendoza, Floreana
Miesen, David Morche, Agostina Ortiz, and Simon Terweh for their help during field work.

References

750   Aizebeokhai, A. P. and Oyeyemi, K. D.: The use of the multiple-gradient array for geoelectrical resistivity and induced polarization
imaging, J Appl Geophys, 111, 364-376, https://doi.org/10.1016/j.jappgeo.2014.10.023, 2014.

Archie, G. E.: The Electrical Resistivity Log as an Aid in Determining Some Reservoir Characteristics, SPE-942054-G, 146, 54-62,
10.2118/942054-G, 1942.

Arenson, L., Hoelzle, M., and Springman, S.: Borehole deformation measurements and internal structure of some rock glaciers in
755   Switzerland, Permafrost and Periglacial Processes, 13, 117-135, Doi 10.1002/Ppp.414, 2002.

Arenson, L. U. and Jakob, M.: The Significance of Rock Glaciers in the Dry Andes - A Discussion of Azocar and Brenning (2010) and
Brenning and Azocar (2010), Permafrost and Periglacial Processes, 21, 282-285, Doi 10.1002/Ppp.693, 2010.

Azocar, G. F. and Brenning, A.: Hydrological and Geomorphological Significance of Rock Glaciers in the Dry Andes, Chile (27 degrees-
33 degrees S), Permafrost and Periglacial Processes, 21, 42-53, Doi 10.1002/Ppp.669, 2010.

760   Barnett, T. P., Adam, J. C., and Lettenmaier, D. P.: Potential impacts of a warming climate on water availability in snow-dominated
regions, Nature, 438, 303-309, 2005.

Barsch, D.: Rockglaciers: indicators for the present and former geoecology in high mountain environments, Springer, 1996.

Berthling, I.: Beyond confusion: Rock glaciers as cryo-conditioned landforms, Geomorphology, 131, 98-106,
http://dx.doi.org/10.1016/j.geomorph.2011.05.002, 2011.

765   Blöthe, J. H., Rosenwinkel, S., Höser, T., and Korup, O.: Rock-glacier dams in High Asia, Earth Surf Proc Land, 44, 808-824,
10.1002/esp.4532, 2019.

Bookhagen, B. and Burbank, D. W.: Topography, relief, and TRMM-derived rainfall variations along the Himalaya, Geophys Res Lett, 33,
10.1029/2006GL026037, 2006.

Bradley, R. S., Vuille, M., Diaz, H. F., and Vergara, W.: Threats to water supplies in the tropical Andes, Science, 312, 1755-1756, 2006.

770   Brasington, J., Langham, J., and Rumsby, B.: Methodological sensitivity of morphometric estimates of coarse fluvial sediment transport,
Geomorphology, 53, 299-316, https://doi.org/10.1016/S0169-555X(02)00320-3, 2003.

Braun, M. H., Malz, P., Sommer, C., Farías-Barahona, D., Sauter, T., Casassa, G., Soruco, A., Skvarca, P., and Seehaus, T. C.:
Constraining glacier elevation and mass changes in South America, Nat Clim Change, 9, 130-136, 10.1038/s41558-018-0375-7, 2019.

Brenning, A.: Geomorphological, hydrological and climatic significance of rock glaciers in the Andes of Central Chile (33-35 degrees S),
775   Permafrost and Periglacial Processes, 16, 231-240, Doi 10.1002/Ppp.528, 2005.

Brenning, A.: The significance of rock glaciers in the dry Andes – reply to L. Arenson and M. Jakob, Permafrost and Periglacial Processes,
21, 286-288, 10.1002/ppp.702, 2010.

Buchli, T., Kos, A., Limpach, P., Merz, K., Zhou, X., and Springman, S. M.: Kinematic investigations on the Furggwanghorn Rock
Glacier, Switzerland, Permafrost and Periglacial Processes, 29, 3-20, 10.1002/ppp.1968, 2018.

780   Burger, K. C., Degenhardt Jr, J. J., and Giardino, J. R.: Engineering geomorphology of rock glaciers, Geomorphology, 31, 93-132, http://dx.doi.org/10.1016/S0169-555X(99)00074-4, 1999.

CEAZA: Datos provistos por CEAZA, obtenidos desde www.ceazamet.cl, 2019. 2019.

Cicoira, A., Beutel, J., Faillettaz, J., and Vieli, A.: Water controls the seasonal rhythm of rock glacier flow, Earth Planet Sc Lett, 528, 115844, https://doi.org/10.1016/j.epsl.2019.115844, 2019.

785   Colombo, N., Salerno, F., Gruber, S., Freppaz, M., Williams, M., Fratianni, S., and Giardino, M.: Review: Impacts of permafrost degradation on inorganic chemistry of surface fresh water, Global Planet Change, 162, 69-83, 2018a.

Colombo, N., Sambuelli, L., Comina, C., Colombero, C., Giardino, M., Gruber, S., Viviano, G., Antisari, L. V., and Salerno, F.: Mechanisms linking active rock glaciers and impounded surface water formation in high-mountain areas, Earth Surf Proc Land, 43, 417-431, 10.1002/esp.4257, 2018b.

790   Corte, A.: The Hydrological Significance of Rock Glaciers, J Glaciol, 17, 157-158, 10.3189/S0022143000030859, 1976.

Corte, A.: Rock glaciers as permafrost bodies with a debris cover as an active layer. A hydrological approach, Andes of Mendoza, Argentina, 1978, 262-269.

Croce, F. A. and Milana, J. P.: Internal structure and behaviour of a rock glacier in the Arid Andes of Argentina, Permafrost and Periglacial Processes, 13, 289-299, 10.1002/ppp.431, 2002.

795   Cuffey, K. M. and Paterson, W. S. B.: The physics of glaciers, Academic Press, 2010.

Dahlin, T. and Zhou, B.: A numerical comparison of 2D resistivity imaging with 10 electrode arrays, Geophys Prospect, 52, 379-398, 10.1111/j.1365-2478.2004.00423.x, 2004.

Dall'Asta, E., Forlani, G., Roncella, R., Santise, M., Diotri, F., and Morra di Cella, U.: Unmanned Aerial Systems and DSM matching for rock glacier monitoring, Isprs J Photogramm, 127, 102-114, https://doi.org/10.1016/j.isprsjprs.2016.10.003, 2017.

800   Draebing, D.: Application of refraction seismics in alpine permafrost studies: A review, Earth-Sci Rev, 155, 136-152, 10.1016/j.earscirev.2016.02.006, 2016.

Drewes, J., Moreiras, S., and Korup, O.: Permafrost activity and atmospheric warming in the Argentinian Andes, Geomorphology, 323, 13-24, https://doi.org/10.1016/j.geomorph.2018.09.005, 2018.

805   Duguay, M. A., Edmunds, A., Arenson, L. U., and Wainstein, P. A.: Quantifying the significance of the hydrological contribution of a rock glacier–A review. In: GEOQuébec 2015: Challenges From North to South, Québec, Canada, 2015.

Dussaillant, I., Berthier, E., Brun, F., Masiokas, M., Hugonnet, R., Favier, V., Rabatel, A., Pitte, P., and Ruiz, L.: Two decades of glacier mass loss along the Andes, Nat Geosci, 12, 802-808, 10.1038/s41561-019-0432-5, 2019.

Duvillard, P. A., Revil, A., Qi, Y., Soueid Ahmed, A., Coperey, A., and Ravanel, L.: Three-Dimensional Electrical Conductivity and Induced Polarization Tomography of a Rock Glacier, Journal of Geophysical Research: Solid Earth, 123, 9528-9554,
810   10.1029/2018JB015965, 2018.

Emmert, A. and Kneisel, C.: Internal structure of two alpine rock glaciers investigated by quasi-3-D electrical resistivity imaging, The Cryosphere, 11, 841-855, 10.5194/tc-11-841-2017, 2017.

Förstner, W.: A feature based correspondence algorithm for image matching, International Archives of Photogrammetry and Remote Sensing, 26, 150-166, 1986.

815   Geiger, S. T., Daniels, J. M., Miller, S. N., and Nicholas, J. W.: Influence of rock glaciers on stream hydrology in the La Sal Mountains, Utah, Arct Antarct Alp Res, 46, 645-658, Doi 10.1657/1938-4246-46.3.645, 2014.

Haeberli, W., Hallet, B., Arenson, L., Elconin, R., Humlun, O., Kaab, A., Kaufmann, V., Ladanyi, B., Matsuoka, N., Springman, S., and Vonder Muhll, D.: Permafrost creep and rock glacier dynamics, Permafrost and Periglacial Processes, 17, 189-214, 10.1002/ppp.561, 2006.

820   Haeberli, W., Hoelzle, M., Kääb, A., Keller, F., Vonder Mühll, D., and Wagner, S.: Ten years after drilling through the permafrost of the active rock glacier Murtèl, Eastern Swiss Alps: answered questions and new perspectives, 1998, 403-410.

Harrington, J. S., Hayashi, M., and Kurylyk, B. L.: Influence of a rock glacier spring on the stream energy budget and cold-water refuge in an alpine stream, Hydrol Process, 31, 4719-4733, 10.1002/hyp.11391, 2017.

Harrington, J. S., Mozil, A., Hayashi, M., and Bentley, L. R.: Groundwater flow and storage processes in an inactive rock glacier, Hydrol
825   Process, 32, 3070-3088, 2018.

Hauck, C.: New Concepts in Geophysical Surveying and Data Interpretation for Permafrost Terrain, Permafrost and Periglacial Processes, 24, 131-137, 10.1002/ppp.1774, 2013.

Hauck, C., Bottcher, M., and Maurer, H.: A new model for estimating subsurface ice content based on combined electrical and seismic data sets, Cryosphere, 5, 453-468, DOI 10.5194/tc-5-453-2011, 2011.

830   Hauck, C. and Kneisel, C.: Applied Geophysics in Periglacial Environments, Cambridge University Press, 2008.

Hausmann, H., Krainer, K., Bruckl, E., and Mostler, W.: Internal structure and ice content of reichenkar rock glacier (Stubai alps, Austria) assessed by geophysical investigations, Permafrost and Periglacial Processes, 18, 351-367, Doi 10.1002/Ppp.601, 2007.

Hausmann, H., Krainer, K., Bruckl, E., and Ullrich, C.: Internal Structure, Ice Content and Dynamics of Olgrube and Kaiserberg Rock Glaciers (Otztal Alps, Austria) Determined from Geophysical Surveys, Austrian J Earth Sci, 105, 12-31, 2012.

835   Heredia, N., Farias, P., García-Sansegundo, J., and Giambiagi, L.: The basement of the Andean Frontal Cordillera in the Cordón del Plata (Mendoza, Argentina): Geodynamic evolution, Andean Geol, 39, 242-257, http://dx.doi.org/10.5027/andgeoV39n2-a03, 2012.

Heredia, N., Rodríguez Fernández, L. R., Gallastegui, G., Busquets, P., and Colombo, F.: Geological setting of the Argentine Frontal Cordillera in the flat-slab segment (30°00′–31°30′S latitude), J S Am Earth Sci, 15, 79-99, https://doi.org/10.1016/S0895-9811(02)00007-X, 2002.

840   Hilbich, C.: Time-lapse refraction seismic tomography for the detection of ground ice degradation, The Cryosphere, 4, 243-259, 10.5194/tc-4-243-2010, 2010.

Hilbich, C., Hauck, C., Hoelzle, M., Scherler, M., Schudel, L., Voelksch, I., Muehll, D. V., and Maeusbacher, R.: Monitoring mountain permafrost evolution using electrical resistivity tomography: A 7-year study of seasonal, annual, and long-term variations at Schilthorn, Swiss Alps, J Geophys Res-Earth, 113, Artn F01s90
845   Doi 10.1029/2007jf000799, 2008.

Hilbich, C., Marescot, L., Hauck, C., Loke, M. H., and Mäusbacher, R.: Applicability of electrical resistivity tomography monitoring to coarse blocky and ice-rich permafrost landforms, Permafrost and Periglacial Processes, 20, 269-284, 10.1002/ppp.652, 2009.

IANIGLA: Data provided by Instituto Argentino de Nivología, Glaciología y Ciencias Ambientales (IANIGLA), "Agua Negra" and "Diaguita" meteorological stations, http://bdhi.hidricosargentina.gob.ar. 2019.

850   IANIGLA: Inventario Nacional de Glaciares. Informe de la subcuenca río Blanco Superior. Cuenca del río Jáchal. IANIGLA-CONICET, Ministerio de Ambiente y Desarrollo Sustentable de la Nación., 65 pp., 2018.

Ikeda, A.: Combination of conventional geophysical methods for sounding the composition of rock glaciers in the Swiss Alps, Permafrost and Periglacial Processes, 17, 35-48, Doi 10.1002/Ppp.550, 2006.

Ikeda, A., Matsuoka, N., and Kaab, A.: Fast deformation of perennially frozen debris in a warm rock glacier in the Swiss Alps: An effect
855   of liquid water, J Geophys Res-Earth, 113, Artn F01021
10.1029/2007jf000859, 2008.

Jones, D. B., Harrison, S., Anderson, K., and Betts, R. A.: Mountain rock glaciers contain globally significant water stores, Sci Rep-Uk, 8, 2018a.

Jones, D. B., Harrison, S., Anderson, K., Selley, H. L., Wood, J. L., and Betts, R. A.: The distribution and hydrological significance of
860   rock glaciers in the Nepalese Himalaya, Global Planet Change, 160, 123-142, 10.1016/j.gloplacha.2017.11.005, 2018b.

Jones, D. B., Harrison, S., Anderson, K., and Whalley, W. B.: Rock glaciers and mountain hydrology: A review, Earth-Sci Rev, doi: https://doi.org/10.1016/j.earscirev.2019.04.001, 2019. https://doi.org/10.1016/j.earscirev.2019.04.001, 2019.

Kääb, A., Frauenfelder, R., and Roer, I.: On the response of rockglacier creep to surface temperature increase, Global Planet Change, 56, 172-187, https://doi.org/10.1016/j.gloplacha.2006.07.005, 2007.

865   Kääb, A., Gudmundsson, G. H., and Hoelzle, M.: Surface deformation of creeping mountain permafrost. Photogrammetric investigations on rock glacier Murtèl, Swiss Alps, 1998, 531-537.

Kääb, A., Haeberli, W., and Gudmundsson, G. H.: Analysing the creep of mountain permafrost using high precision aerial photogrammetry: 25 years of monitoring Gruben Rock Glacier, Swiss Alps, Permafrost and Periglacial Processes, 8, 409-426, 1997.

Kääb, A., Kaufmann, V., Ladstädter, R., and Eiken, T.: Rock glacier dynamics: Implications from high-resolution measurements of
870   surface velocity fields, 8th International Conference on Permafrost, Zürich, 501-506, 2003.

Kääb, A. and Weber, M.: Development of transverse ridges on rock glaciers: Field measurements and laboratory experiments, Permafrost and Periglacial Processes, 15, 379-391, 2004.

Kenner, R., Phillips, M., Beutel, J., Hiller, M., Limpach, P., Pointner, E., and Volken, M.: Factors Controlling Velocity Variations at Short-Term, Seasonal and Multiyear Time Scales, Ritigraben Rock Glacier, Western Swiss Alps, Permafrost and Periglacial Processes, 28, 675-684, 10.1002/ppp.1953, 2017.

Kenner, R., Pruessner, L., Beutel, J., Limpach, P., and Phillips, M.: How rock glacier hydrology, deformation velocities and ground temperatures interact: Examples from the Swiss Alps, Permafrost and Periglacial Processes, 0, 10.1002/ppp.2023, 2019.

King, M. S., Zimmerman, R. W., and Corwin, R. F.: Seismic and Electrical Properties of Unconsolidated Permafrost, Geophys Prospect, 36, 349-364, 10.1111/j.1365-2478.1988.tb02168.x, 1988.

Kneisel, C., Hauck, C., Fortier, R., and Moorman, B.: Advances in geophysical methods for permafrost investigations, Permafrost and Periglacial Processes, 19, 157-178, Doi 10.1002/Ppp.616, 2008.

Knight, J., Harrison, S., and Jones, D. B.: Rock glaciers and the geomorphological evolution of deglacierizing mountains, Geomorphology, 324, 14-24, https://doi.org/10.1016/j.geomorph.2018.09.020, 2019.

Konrad, S. K., Humphrey, N. F., Steig, E. J., Clark, D. H., Potter, N., Jr, and Pfeffer, W. T.: Rock glacier dynamics and paleoclimatic implications, Geology, 27, 1131-1134, 10.1130/0091-7613(1999)027<1131:rgdapi>2.3.co;2, 1999.

Krainer, K., Bressan, D., Dietre, B., Haas, J. N., Hajdas, I., Lang, K., Mair, V., Nickus, U., Reidl, D., Thies, H., and Tonidandel, D.: A 10,300-year-old permafrost core from the active rock glacier Lazaun, southern Ötztal Alps (South Tyrol, northern Italy), Quaternary Res, 83, 324-335, 10.1016/j.yqres.2014.12.005, 2017.

Krainer, K. and Mostler, W.: Hydrology of active rock glaciers: Examples from the Austrian Alps, Arct Antarct Alp Res, 34, 142-149, Doi 10.2307/1552465, 2002.

Krainer, K., Mostler, W., and Spötl, C.: Discharge from active rock glaciers, Austrian Alps: a stable isotope approach, Austrian J Earth Sci, 100, 102-112, 2007.

Krautblatter, M. and Draebing, D.: Pseudo 3-D P wave refraction seismic monitoring of permafrost in steep unstable bedrock, Journal of Geophysical Research: Earth Surface, 119, 287-299, 10.1002/2012jf002638, 2014.

Kummert, M., Delaloye, R., and Braillard, L.: Erosion and sediment transfer processes at the front of rapidly moving rock glaciers: Systematic observations with automatic cameras in the western Swiss Alps, Permafrost and Periglacial Processes, 29, 21-33, 2018.

Langston, G., Bentley, L. R., Hayashi, M., McClymont, A., and Pidlisecky, A.: Internal structure and hydrological functions of an alpine proglacial moraine, Hydrol Process, 25, 2967-2982, 10.1002/hyp.8144, 2011.

Lecomte, K. L., Milana, J. P., Formica, S. M., and Depetris, P. J.: Hydrochemical appraisal of ice- and rock-glacier meltwater in the hyperarid Agua Negra drainage basin, Andes of Argentina, Hydrol Process, 22, 2180-2195, Doi 10.1002/Hyp.6816, 2008.

Loke, M. H.: Tutorial : 2-D and 3-D electrical imaging surveys, 2018. 2018.

Luethi, R., Phillips, M., and Lehning, M.: Estimating Non-Conductive Heat Flow Leading to Intra-Permafrost Talik Formation at the Ritigraben Rock Glacier (Western Swiss Alps), Permafrost and Periglacial Processes, 28, 183-194, 10.1002/ppp.1911, 2017.

Malmros, J. K., Mernild, S. H., Wilson, R., Tagesson, T., and Fensholt, R.: Snow cover and snow albedo changes in the central Andes of Chile and Argentina from daily MODIS observations (2000–2016), Remote Sens Environ, 209, 240-252, https://doi.org/10.1016/j.rse.2018.02.072, 2018.

Marescot, L., Loke, M., Chapellier, D., Delaloye, R., Lambiel, C., and Reynard, E.: Assessing reliability of 2D resistivity imaging in mountain permafrost studies using the depth of investigation index method, Near Surf Geophys, 1, 57-67, 2003.

Marmy, A., Rajczak, J., Delaloye, R., Hilbich, C., Hoelzle, M., Kotlarski, S., Lambiel, C., Noetzli, J., Phillips, M., Salzmann, N., Staub, B., and Hauck, C.: Semi-automated calibration method for modelling of mountain permafrost evolution in Switzerland, The Cryosphere, 10, 2693-2719, 10.5194/tc-10-2693-2016, 2016.

Maurer, H. and Hauck, C.: Instruments and methods - Geophysical imaging of alpine rock glaciers, J Glaciol, 53, 110-120, Doi 10.3189/172756507781833893, 2007.

McClymont, A. F., Hayashi, M., Bentley, L. R., and Liard, J.: Locating and characterising groundwater storage areas within an alpine watershed using time-lapse gravity, GPR and seismic refraction methods, Hydrol Process, 26, 1792-1804, Doi 10.1002/Hyp.9316, 2012.

McClymont, A. F., Hayashi, M., Bentley, L. R., Muir, D., and Ernst, E.: Groundwater flow and storage within an alpine meadow-talus complex, Hydrol Earth Syst Sc, 14, 859-872, 2010.

Mewes, B., Hilbich, C., Delaloye, R., and Hauck, C.: Resolution capacity of geophysical monitoring regarding permafrost degradation induced by hydrological processes, Cryosphere, 11, 2957-2974, 2017.

920   Milana, J. P. and Maturano, A.: Application of Radio Echo Sounding at the arid Andes of Argentina: the Agua Negra Glacier, Global
        Planet Change, 22, 179-191, Doi 10.1016/S0921-8181(99)00035-1, 1999.

        Mollaret, C., Hilbich, C., Pellet, C., Flores-Orozco, A., Delaloye, R., and Hauck, C.: Mountain permafrost degradation documented
        through a network of permanent electrical resistivity tomography sites, The Cryosphere, 13, 2557-2578, 10.5194/tc-13-2557-2019, 2019.

        Monnier, S. and Kinnard, C.: Internal structure and composition of a rock glacier in the Andes (upper Choapa valley, Chile) using
925   borehole information and ground-penetrating radar, Ann. Glaciol., 54, 61-72, Doi 10.3189/2013aog64a107, 2013.

        Mosbrucker, A. R., Major, J. J., Spicer, K. R., and Pitlick, J.: Camera system considerations for geomorphic applications of SfM
        photogrammetry, Earth Surf Proc Land, 42, 969-986, 2017.

        Musil, M., Maurer, H., Green, A. G., Horstmeyer, H., Nitsche, F. O., Vonder Muhll, D., and Springman, S.: Shallow seismic surveying of
        an Alpine rock glacier, Geophysics, 67, 1701-1710, Doi 10.1190/1.1527071, 2002.

930   Otto, J. C. and Sass, O.: Comparing geophysical methods for talus slope investigations in the Turtmann valley (Swiss Alps),
        Geomorphology, 76, 257-272, 2006.

        Pellet, C., Hilbich, C., Marmy, A., and Hauck, C.: Soil Moisture Data for the Validation of Permafrost Models Using Direct and Indirect
        Measurement Approaches at Three Alpine Sites, Frontiers in Earth Science, 3, 10.3389/feart.2015.00091, 2016.

        Rangecroft, S., Harrison, S., and Anderson, K.: Rock Glaciers as Water Stores in the Bolivian Andes: An Assessment of Their
935   Hydrological Importance, Arctic, Antarctic, and Alpine Research, 47, 89-98, 10.1657/AAAR0014-029, 2015.

        Rangecroft, S., Suggitt, A. J., Anderson, K., and Harrison, S.: Future climate warming and changes to mountain permafrost in the Bolivian
        Andes, Climatic Change, 137, 231-243, 10.1007/s10584-016-1655-8, 2016.

        Rogger, M., Chirico, G. B., Hausmann, H., Krainer, K., Brückl, E., Stadler, P., and Blöschl, G.: Impact of mountain permafrost on flow
        path and runoff response in a high alpine catchment, Water Resour Res, 53, 1288-1308, 10.1002/2016WR019341, 2017.

940   Saavedra, F. A., Kampf, S. K., Fassnacht, S. R., and Sibold, J. S.: Changes in Andes snow cover from MODIS data, 2000–2016, The
        Cryosphere, 12, 1027-1046, 10.5194/tc-12-1027-2018, 2018.

        Sandmeier, K. J.: ReflexW version 8.0. Program for the Processing of Seismic, Acoustic or Electromagnetic Reflection, Refraction and
        Transmission Data, User's Manual, 2016. 578, 2016.

        Schaffer, N., MacDonell, S., Réveillet, M., Yáñez, E., and Valois, R.: Rock glaciers as a water resource in a changing climate in the
945   semiarid Chilean Andes, Reg Environ Change, doi: 10.1007/s10113-018-01459-3, 2019. 10.1007/s10113-018-01459-3, 2019.

        Scherler, M., Hauck, C., Hoelzle, M., and Salzmann, N.: Modeled sensitivity of two alpine permafrost sites to RCM-based climate
        scenarios, J Geophys Res-Earth, 118, 780-794, Doi 10.1002/Jgrf.20069, 2013.

        Scherler, M., Hauck, C., Hoelzle, M., Stahli, M., and Volksch, I.: Meltwater Infiltration into the Frozen Active Layer at an Alpine
        Permafrost Site, Permafrost and Periglacial Processes, 21, 325-334, Doi 10.1002/Ppp.694, 2010.

950   Schneider, S., Daengeli, S., Hauck, C., and Hoelzle, M.: A spatial and temporal analysis of different periglacial materials by using
        geoelectrical, seismic and borehole temperature data at Murtèl–Corvatsch, Upper Engadin, Swiss Alps, Geogr. Helv., 68, 265-280,
        10.5194/gh-68-265-2013, 2013.

        Schön, J.: Physical properties of rocks: A workbook, Elsevier, 2011.

        Schrott, L.: Die Solarstrahlung als steuernder Faktor im Geosystem der subtropischen semiariden Hochanden (Agua Negra, San Juan,
955   Argentinien), 1994. Geographisches Inst. der Univ. Heidelberg, Heidelberg, 1994.

        Schrott, L.: Global solar radiation, soil temperature and permafrost in the Central Andes, Argentina: A progress report, Permafrost and
        Periglacial Processes, 2, 59-66, 10.1002/ppp.3430020110, 1991.

        Schrott, L.: The hydrological significance of high mountain permafrost and its relation to solar radiation, A case study in the high Andes of
        San Juan, Argentina. Bamberger Geographische Schriften, Bd, 15, 71-84, 1998.

960   Schrott, L.: Some geomorphological-hydrological aspects of rock glaciers in the Andes (San Juan, Argentina), Z. Geomorph. N.F., Suppl.-
        Bd. 104, 1996.

        Schrott, L. and Hoffmann, T.: Refraction seismics. In: Applied Geophysics in Periglacial Environments, Hauck, C. and Kneisel, C. (Eds.),
        Cambridge University Press, Cambridge, 2008.

        Schwalbe, E. and Maas, H. G.: The determination of high-resolution spatio-temporal glacier motion fields from time-lapse sequences,
965   Earth Surf. Dynam., 5, 861-879, 10.5194/esurf-5-861-2017, 2017.

Springman, S. M., Arenson, L. U., Yamamoto, Y., Maurer, H., Kos, A., Buchli, T., and Derungs, G.: Multidisciplinary Investigations on Three Rock Glaciers in the Swiss Alps: Legacies and Future Perspectives, Geogr Ann A, 94A, 215-243, DOI 10.1111/j.1468-0459.2012.00464.x, 2012.

970   Tapia-Baldis, C. and Trombotto-Liaudat, D.: Permafrost model in coarse-blocky deposits for the Dry Andes, Argentina (28°-33° S), Cuadernos de Investigación Geográfica 46, doi: http://dx.doi.org/10.18172/cig.3802, 2020. http://dx.doi.org/10.18172/cig.3802, 2020.

Timur, A.: Velocity of Compressional Waves in Porous Media at Permafrost Temperatures, Geophysics, 33, 584-&, Doi 10.1190/1.1439954, 1968.

Trombotto, D. and Borzotta, E.: Indicators of present global warming through changes in active layer-thickness, estimation of thermal diffusivity and geomorphological observations in the Morenas Coloradas rockglacier, Central Andes of Mendoza, Argentina, Cold Reg Sci
975   Technol, 55, 321-330, DOI 10.1016/j.coldregions.2008.08.009, 2009.

Trombotto, D., Buk, E., and Hernández, J.: Rock glaciers in the Southern Central Andes (approx. 33–34S), Cordillera Frontal, Mendoza, Argentina, Bamberger Geographische Schriften, 19, 145-173, 1999.

Wheaton, J. M., Brasington, J., Darby, S. E., and Sear, D. A.: Accounting for uncertainty in DEMs from repeat topographic surveys: improved sediment budgets, Earth Surf Proc Land, 35, 136-156, 10.1002/esp.1886, 2010.

980   Williams, M. W., Knauf, M., Caine, N., Liu, F., and Verplanck, P. L.: Geochemistry and source waters of rock glacier outflow, Colorado Front Range, Permafrost and Periglacial Processes, 17, 13-33, Doi 10.1002/Ppp.535, 2006.

Wirz, V., Gruber, S., Purves, R. S., Beutel, J., Gartner-Roer, I., Gubler, S., and Vieli, A.: Short-term velocity variations at three rock glaciers and their relationship with meteorological conditions, Earth Surf Dynam, 4, 103-123, 10.5194/esurf-4-103-2016, 2016.

985   **Tables**

Table 1: Potential mean annual air temperatures (MAAT) of recent years derived from different local meteorological stations of the Upper Agua Negra basin. The altitudes of 4300 and 4500 m a.s.l. correspond to the elevation range of the Dos Lenguas rock glacier, respectively.

Station (altitude)	Year	MAAT [°C] 4300 m asl[*]	MAAT [°C] 4500 m asl[*]	Reference
El Paso rock glacier (4720 m asl)	1990–91	1.8	–0.1	Schrott (1996)
Paso Agua Negra (4774 m asl)	2015	–0.4	–2.3	CEAZA (2019)
Agua Negra (4460 m asl)	2016	–2.5	–4.5	IANIGLA (2019)
Diaguita (3880 m asl)	2017	–1.1	–3.1	IANIGLA (2019)
Diaguita (3880 m asl)	2018	–0.5	–2.5	IANIGLA (2019)

[*] A dry adiabatic lapse rate of 0.98°C km^{-1} was used to derive potential MAAT in different elevations from each station.

990

Table 2: Details of the ERT surveys (cf. Fig. 1b for position of the profiles).

ERT profiles Dos Lenguas	Orientation	Length [m]	Electrode spacing [m]	Acquisition date	Number of data points Collected	Used	Abs. error after 5 iterations [%]
C1 (cross-profile) Root zone	NNW→SSE	320	4	23rd Feb 2017	1160	992 (86%)	6,2
C2 (cross-profile) Central part	N→S	400	5	27th Feb 2017	1168	1075 (92%)	5,1
L1 (long. profile) Northern tongue	ENE→WSW	240	3	2nd Mar 2017	1168	1117 (96%)	6,7
L2 (long. profile) Southern tongue	NE→SW	400	5	2nd Mar 2018	951	919 (97%)	7,4

Table 3: Details of the SRT surveys. Sensor spacing and orientation of all SRT profiles is identical to the corresponding ERT profiles (cf. Table 2).

SRT profiles Dos Lenguas	Geophone positions on ERT profile [m]	Acquisition date	Shot points	Iterations	RMS deviation [ms]	Total absolute time difference [ms]
C1 (cross-profile) Root zone	20–304	24th Feb 2017	25	9	2.7	2.0
C2 (cross-profile) Central part	20-360	28th Feb 2017	25	14	4.7	3.8
L1 (long. profile) Northern tongue	6-213	3rd Mar 2017	25	13	3.2	2.4
L2 (long. profile) Southern tongue	0-400	3rd Mar 2018	43	11	2.6	2.0

995

Table 4: Model parameters for 4PM calculation.

Prescribed 4PM parameters	
a	1
m	2
n	2
v_w (m s^{-1})	1500
v_r (m s^{-1})	6000
v_i (m s^{-1})	3500
v_a (m s^{-1})	330
Values for model scenarios	
ρ_w (Ω m)	30; 50; 100; 200
$\Phi_{uniform}$	0.3, 0.5, 0.7
*Φ_{mixed}	0.75-0.03
**$\Phi_{active\ layer}$	0.45-0.3
**$\Phi_{Permafrost}$	0.75-0.3
**$\Phi_{bedrock}$	0.1-0.03

*Mixed model includes different porosities of active layer, permafrost and bedrock

**Porosity ranges include depth gradient

1000

Table 5: (top) Level of detection (LoD) is given for different confidence intervals and t-values for detected vertical changes. (bottom) Associated net balance estimates derived from the sum of positive and negative interannual volumetric changes for the observation periods. The net changes are given in water equivalent per year for the whole surface area and each geomorphological unit of the rock glacier. The net balance approximations correspond to interannual water storage change under the assumption that the volumetric changes were mainly caused by gains and losses of ice.

Confidence interval	70%	80%	90%	95%	99%
t-value	1.036	1.282	1.645	1.96	2.576
LoD 2016 – 2017 [m]	0.232	0.287	0.368	0.438	0.576
LoD 2017 – 2018 [m]	0.073	0.091	0.117	0.139	0.183

Net change of positive and negative volumetric changes for the observation periods [mm yr^{-1}]										
Period	2016-17	2017-18	2016-17]	2017-18	2016-17	2017-18	2016-17	2017-18	2016-17	2017-18
Rock glacier surface	-109	+29	-86	+28	-55	+28	-36	+27	-15	+25
Root area	-116	+8	-89	+7	-49	+5	-27	+4	-9	+1
Central part	-141	+15	-117	+15	-84	+14	-61	+14	-33	+14
Northern tongue	-90	+50	-68	+49	-38	+46	-23	+45	-7	+42
Southern tongue	-95	+30	-74	+30	-47	+30	-30	+30	-13	+30

1005

Table 6: Mean fractions of ice, water and air contents for different scenarios containing the minimum and maximum model for ice and water contents, and the scenario with mixed porosities for the anticipated internal structure and pore water resistivities from field measurements. The mean fractions are solely based on model cells below the rock glacier surface area (model area outside the rock glacier were excluded). The ratio of numerically solved model cells to the total model domain gives the amount of physical consistent solutions of the different 4PM scenarios. Absolute ice and water contents are estimated based on mean f_i and f_w along the profiles that were extrapolated to surface area and mean depth of permafrost.

1010

	Model scenarios	Mean f_i [%] [1]	Mean f_w [%] [1]	Mean f_a [%] [1]	Solved model cell ratio [%]	Absolute ice content [10^9 kg] [2]	Absolute water content [10^9 kg] [2]
Cross-profile C1	$\Phi = 30\%, \rho_w = 200\ \Omega\,m$	12 ±6	13±5	5 ±4	43		
Root zone	$\Phi = 70\%, \rho_w = 30\ \Omega\,m$	48 ±16	8 ±5	14 ±14	88	0.364 (±43%)	0.071 (±32%)
(35,500 m²)	$\Phi_{mixed}, \rho_w = 50\ \Omega\,m$	41 ±16	10 ±5	11 ±11	84	0.262 (±43%)	0.057 (±32%)
Cross-profile C2	$\Phi = 30\%, \rho_w = 200\ \Omega\,m$	9 ±5	14±5	7 ±5	41		
Central part	$\Phi = 70\%, \rho_w = 30\ \Omega\,m$	44 ±17	7 ±4	19 ±16	86	0.729 (±44%)	0.120 (±31%)
(66,600 m²)	$\Phi_{mixed}, \rho_w = 50\ \Omega\,m$	38 ±16	8 ±4	14 ±11	65	0.513 (±43%)	0.105 (±31%)
Long. profile L1	$\Phi = 30\%, \rho_w = 200\ \Omega\,m$	9 ±5	12 ±7	9 ±7	41		
Northern tongue	$\Phi = 70\%, \rho_w = 30\ \Omega\,m$	45 ±16	7 ±5	19 ±16	86	0.694 (±43%)	0.138 (±32%)
(77,100 m²)	$\Phi_{mixed}, \rho_w = 50\ \Omega\,m$	36 ±14	9 ±6	13 ±12	76	0.500 (±41%)	0.108 (±33%)
Long. profile L2	$\Phi = 30\%, \rho_w = 200\ \Omega\,m$	9 ±5	13 ±5	8 ±6	43		
Southern Tongue	$\Phi = 70\%, \rho_w = 30\ \Omega\,m$	42 ±18	7 ±4	21 ±17	88	0.625 (±45%)	0.109 (±31%)
(68,100 m²)	$\Phi_{mixed}, \rho_w = 50\ \Omega\,m$	38 ±13	8 ±4	15 ±11	84	0.466 (±40%)	0.095 (±31%)
Rock glacier						2.00 (±44%)	0.432 (±32%)
(247,300 m²)						1.71 (±42%)	0.359 (±32%)

1 errors as standard deviation

2 errors as propagated uncertainties of f_w and f_i, permafrost thickness and surface area

Figures
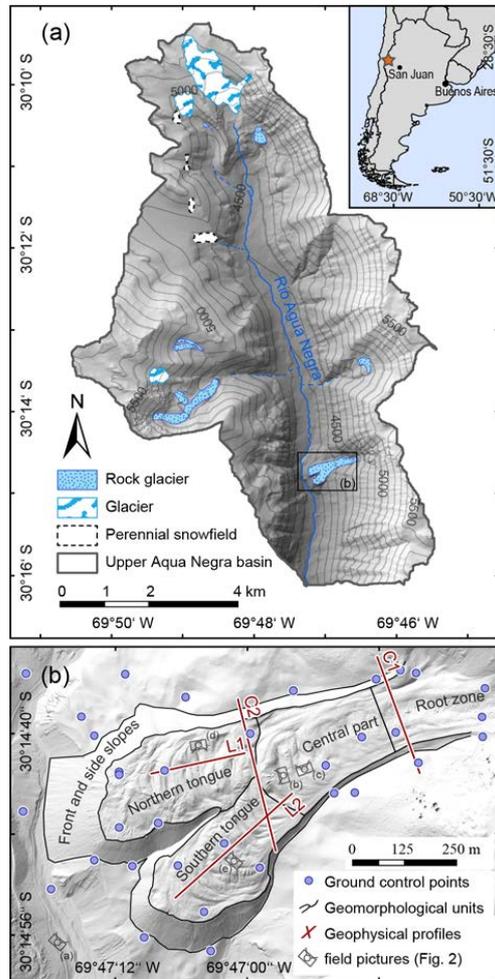
Fig. 1: (a) Spatial distribution of active rock glaciers, glaciers, and perennial snowfields in the Upper Agua Negra catchment (hillshade based on TanDEM-X data © DLR 2017) mapped by the Glacier Inventory of Argentina (IANIGLA, 2018). The inset shows the location of the Upper Agua Negra catchment. (b) Based on the drone-derived DEM 2016, the shaded relief map of Dos Lenguas rock glacier shows the geomorphological units subdivided into root zone, central part, northern and southern tongue, the locations of geophysical profiles, field pictures (Fig. 2), and ground control points, which were used for displacement measurements.
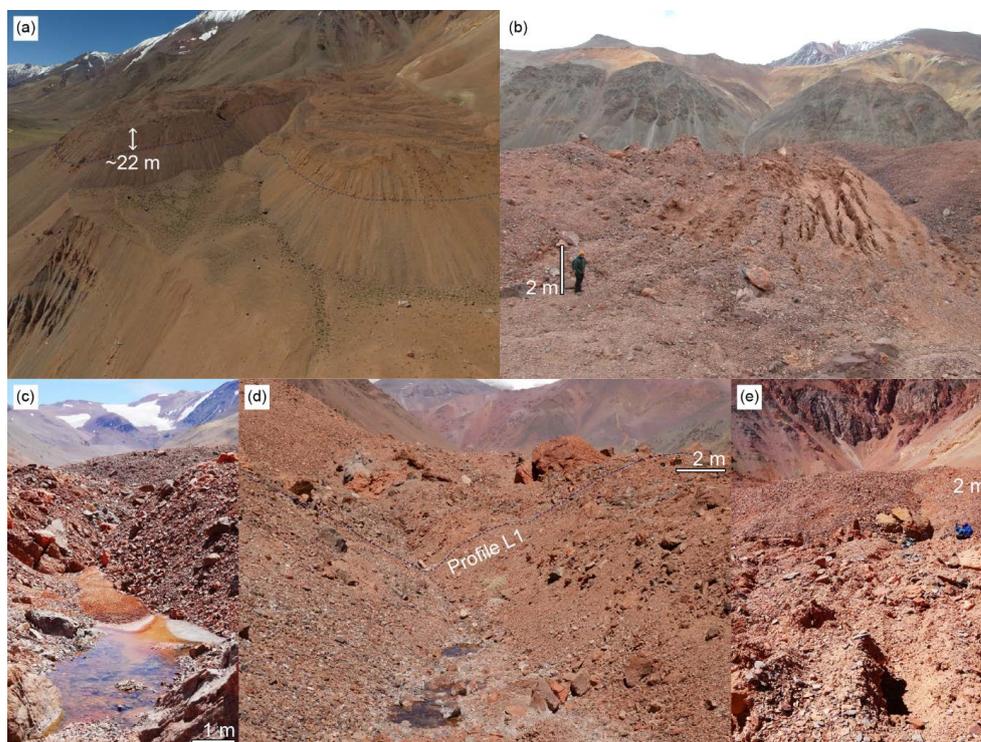
Fig. 2: Field images of Dos Lenguas: (a) View towards the Northern (left) and Southern (right) tongues of the rock glacier. Note gully-like structures in the upper over-steepened frontal slopes indicate the depths of the basal layer at both tongues (dotted lines); **(b)** Crevasses in the central rock glacier part indicate rupturing of transversal ridge thereby exposing fine debris; **(c)** Partly frozen thermokarst pond with delta indicating fine sediment transport and accumulation along water pathways in furrows; **(d)** Thermokarst ponds next to profile L1 on the northern tongue; **(e)** Gully like structures at the surface perpendicular to ridge and furrows indicate meltwater pathways in the active layer next to profile L2 on the southern tongue (larger gullies on the southern tongue are also visible in Figure 1b next to the field image location).
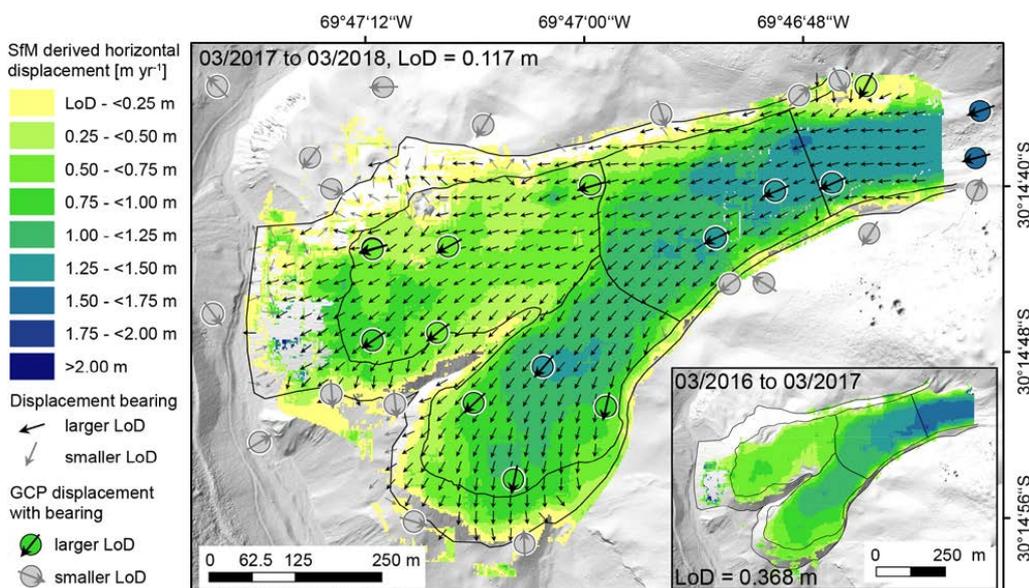
Fig. 3: Horizontal surface displacement on the Dos Lenguas rock glacier.
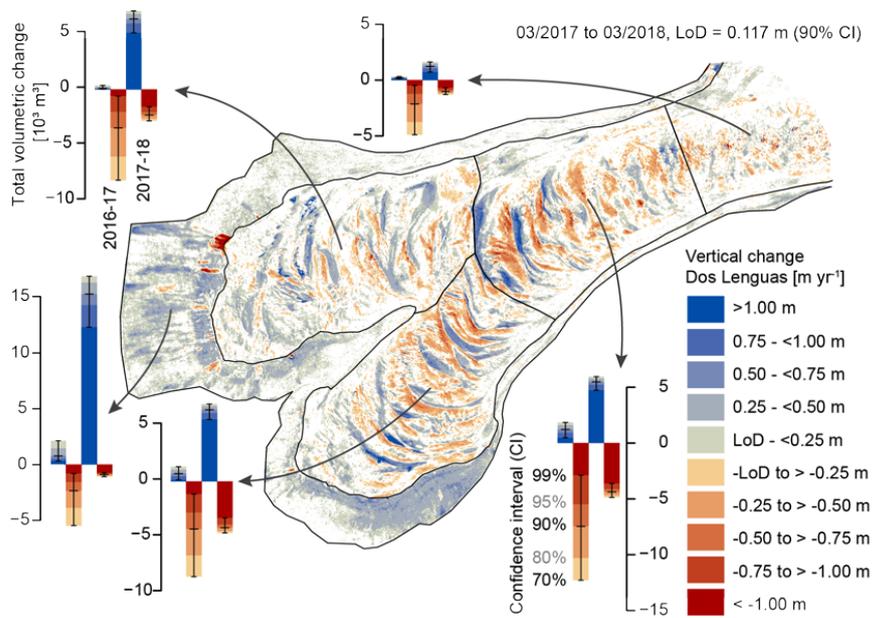
Fig. 4: Volumetric surface changes of Dos Lenguas from 03/2017 to 03/2018. The barplots show positive and negative volumetric changes depending on confidence intervals in different morphological units for the periods 2016-17 and 2017-18. The corresponding net changes of the rock glacier surface are given in Table 5 as water equivalents.

1035
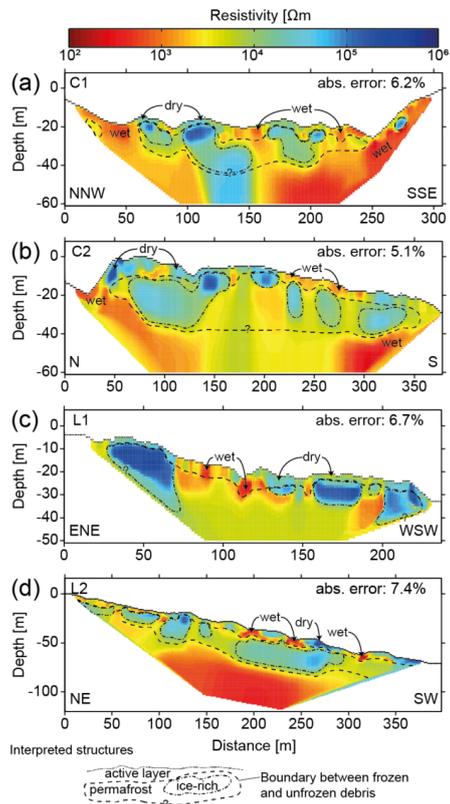
Fig. 5: ERT of Dos Lenguas: a) Cross-profile C1 of the root area, b) Cross-profile C2 of the central rock glacier, c) Long-profile L1 of the Northern tongue, and d) Long-profile L2 of the southern tongue. Note the different horizontal and vertical scales for the different profiles.
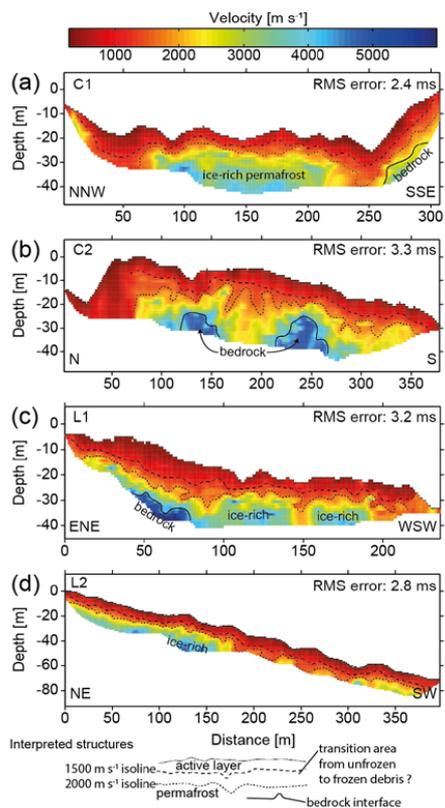
1040

Fig. 6: SRT of Dos Lenguas: a) Cross-profile C1 of the root area, b) Cross-profile C2 of the central rock glacier, c) Long-profile L1 of the Northern tongue, and d) Long-profile L2 of the southern tongue. Note the different horizontal and vertical scales for the different profiles.
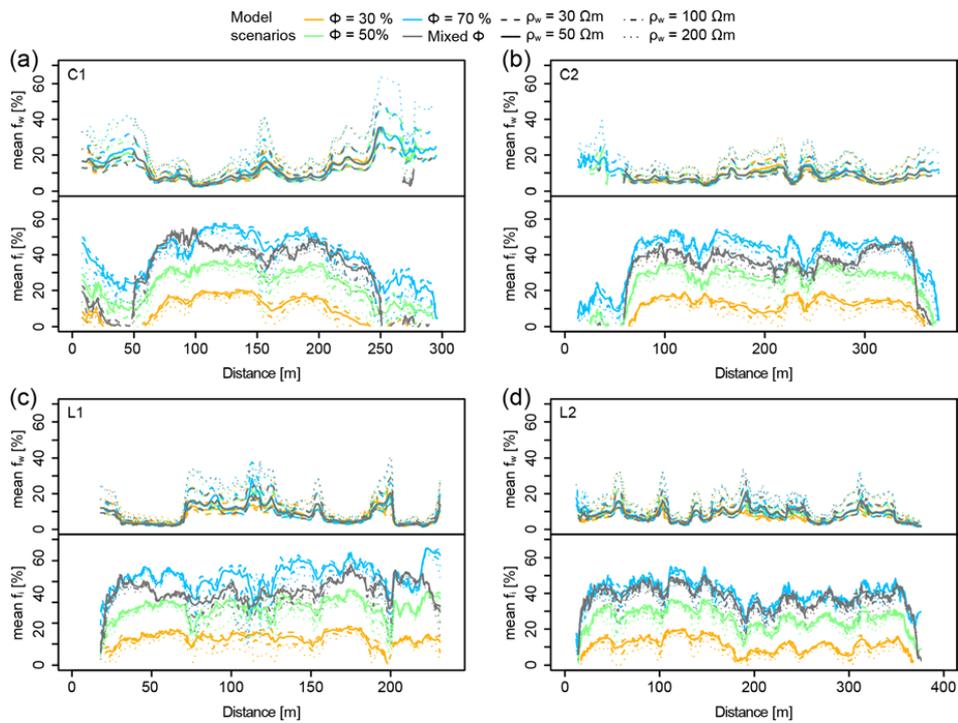
1045   **Fig. 7: Estimated mean ice (f_i) and water (f_w) contents over model depth along the profiles C1, C2, L1 and L2 for all 4PM scenarios.**
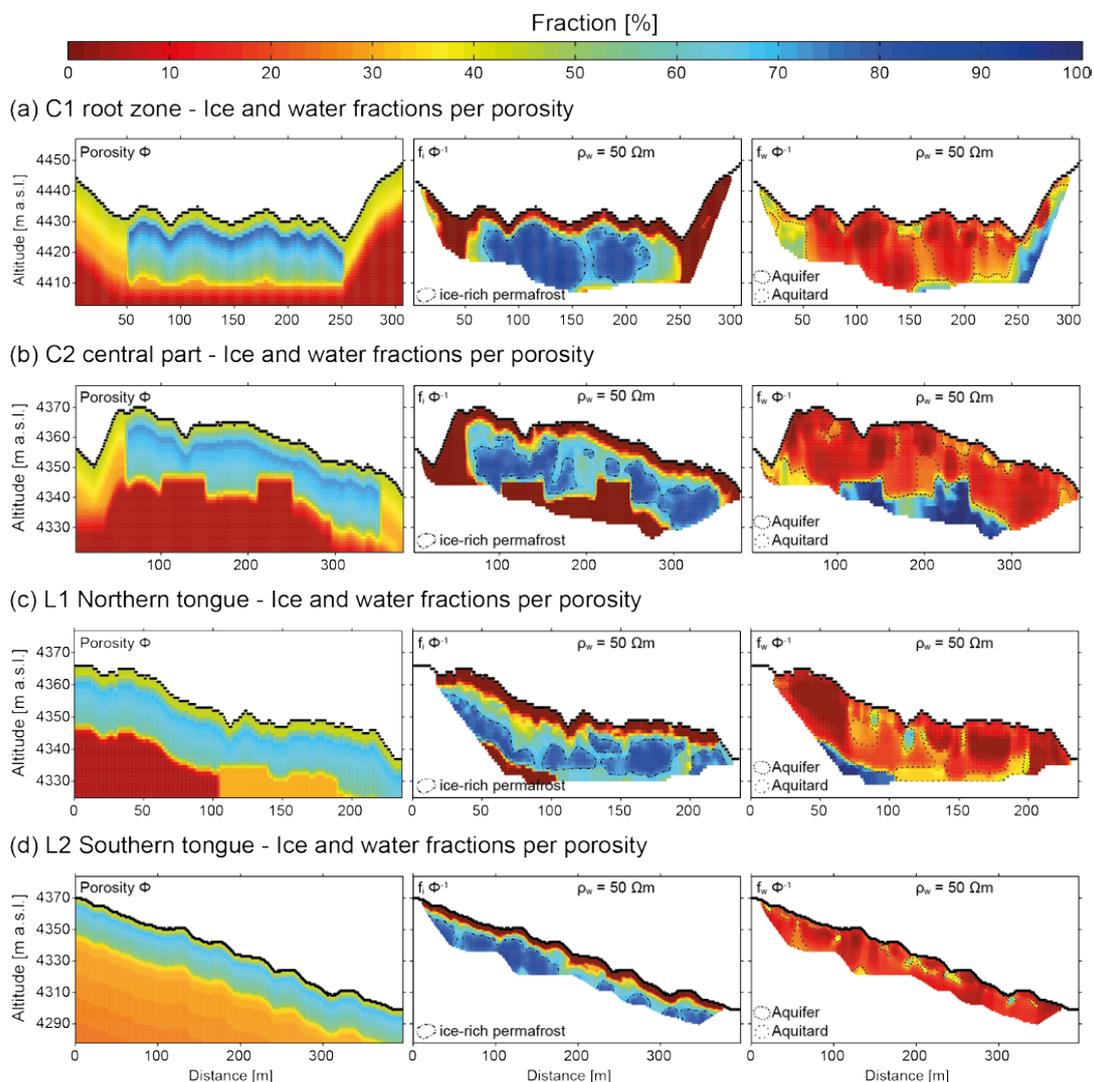
Fig. 8: Spatial distribution of ice and water contents per porosity of the 4PM scenario with mixed porosity model and pore water
resistivities of 50 Ω m for (a) cross-profile C1 in the root zone, (b) cross-profile C2 in the central rock glaciers area, (c) long-profile
L1 in the northern tongue and (d) long-profile L2 in the Southern tongue. Porosities <10% represent potential bedrock occurrence
based on SRT interpretations. Porosities >40% allow ice-rich permafrost conditions in the 4PM. Ice content per porosity ($f_i \Phi^{-1}$)
shows heterogeneous distributions of ice-rich permafrost and indicates the active layer in ice free model cells. High water content
per porosity ($f_w \Phi^{-1}$) indicates water pathways and traps in unfrozen aquifers, while increased water contents between ice-rich
permafrost could indicate aquitards and/or thawing permafrost in late summer. Note the different horizontal and vertical scales of
the figures for the different profiles.
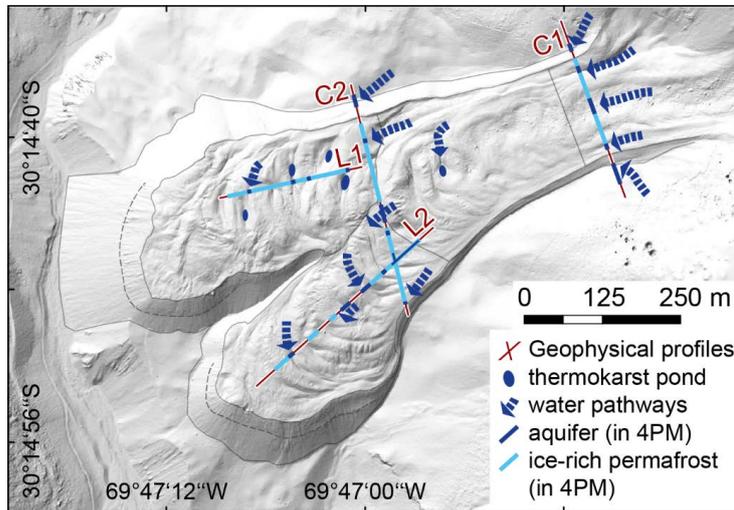
Fig. 9: Topographic positions of aquifers and ice-rich permafrost based on observed hydrological structures in the 4PM along the geophysical profiles (cf. Fig.8). The spatial distribution of ice-rich permafrost, thermokarst ponds, aquifers and interpreted water pathways indicate interrelations with the ridge and furrows topography of Dos Lenguas. The dotted lines show the depth of the basal layers at both front slopes, which roughly corresponds to the thickness of ice-rich permafrost in the tongues.

1060
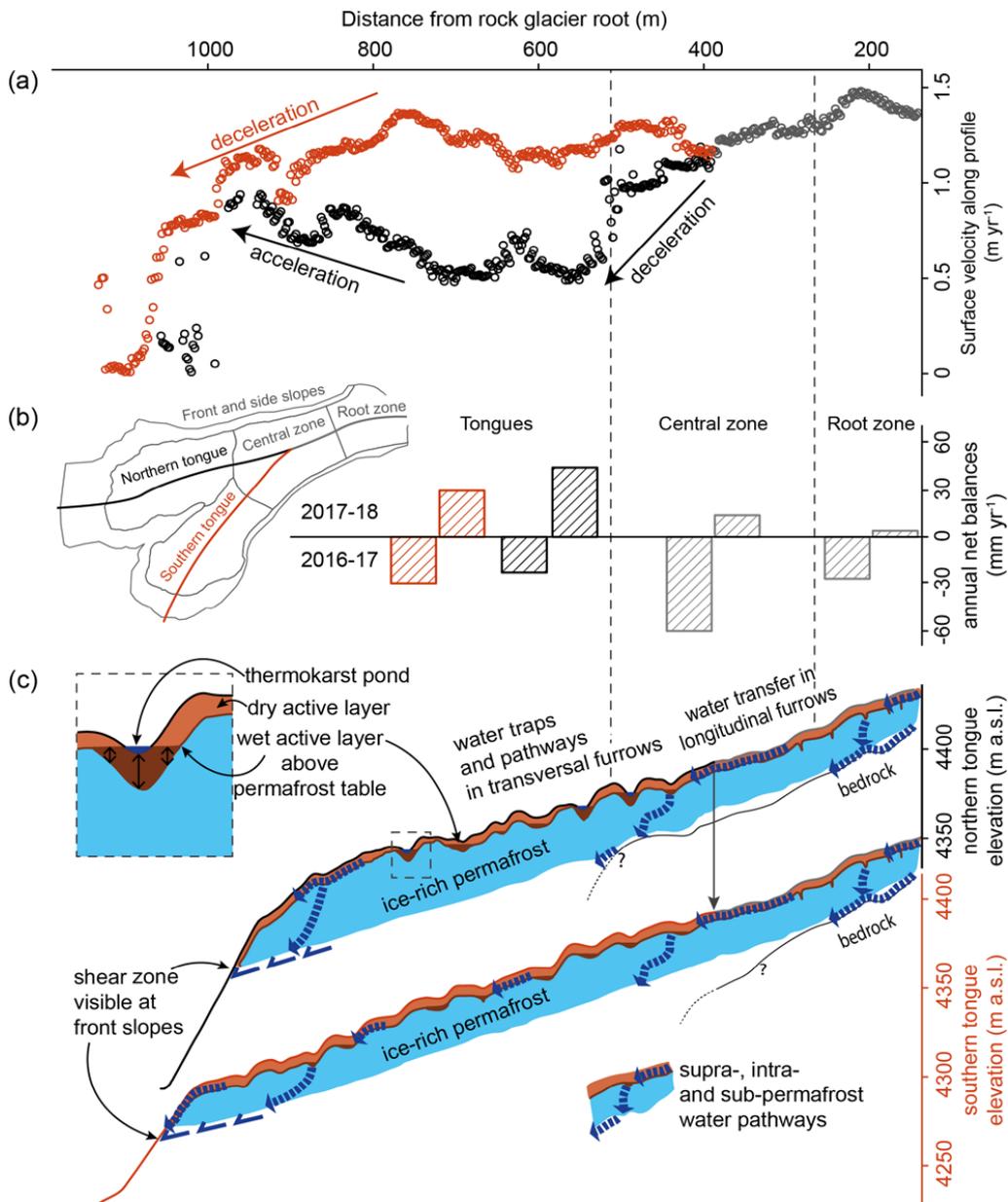
Fig. 10: (a) Spatial interrelation of horizontal surface velocities along the central flow line, (b) negative and positive interannual storage changes (net balance) in 2016–17 and 2017–18, respectively, and (c) longitudinal sketch profiles (not to scale) along the central flowline topographies (scaled) of the northern (black) and southern tongue (red) including potential internal hydrologic structure with water traps and pathways in the active layer, as well as potential intra- and sub-permafrost drainage pathways. Volumetric chances due to seasonal freezing and thawing at the interface of an ice-rich permafrost table and a wet active layer base could be locally enhanced by increased water contents where melt water is trapped in and along furrows e.g. thermokarst ponds (see inset).

1065